HHS Public Access

Author manuscript

Cell Rep. Author manuscript; available in PMC 2022 April 22.

Published in final edited form as:

Cell Rep. 2022 April 05; 39(1): 110587. doi:10.1016/j.celrep.2022.110587.

Developmental maturation of the hematopoietic system controlled by a Lin28b-*let-7*-Cbx2 axis

Dahai Wang[1,9], **Mayuri Tanaka-Yano**[1,9], **Eleanor Meader**[2], **Melissa A. Kinney**[3], **Vivian Morris**[2], **Edroaldo Lummertz da Rocha**[4], **Nan Liu**[1], **Tianxin Liu**[1], **Qian Zhu**[1], **Stuart H. Orkin**[1,5,6,7], **Trista E. North**[2,6], **George Q. Daley**[1,2,6], **R. Grant Rowe**[1,2,6,7,8,10,*]

[1]Department of Hematology/Oncology, Boston Children's Hospital, Boston, MA 02115, USA

[2]Stem Cell Program, Boston Children's Hospital, Boston, MA 02115, USA

[3]Department of Biomedical Engineering, University of Wisconsin-Madison, Madison, WI 53706, USA

[4]Department of Microbiology, Immunology, and Parasitology, Federal University of Santa Catarina, Florianopolis 88040-900, Brazil

[5]Howard Hughes Medical Institute, Boston, MA 02115, USA

[6]Harvard Medical School, Boston, MA 02115, USA

[7]Dana-Farber Boston Children's Cancer and Blood Disorders Center, Boston, MA 02115, USA

[8]Stem Cell Transplantation Program, Boston Children's Hospital, Boston, MA 02115, USA

[9]These authors contributed equally

[10]Lead contact

SUMMARY

Hematopoiesis changes over life to meet the demands of maturation and aging. Here, we find that the definitive hematopoietic stem and progenitor cell (HSPC) compartment is remodeled from gestation into adulthood, a process regulated by the heterochronic Lin28b/*let-7* axis. Native fetal and neonatal HSPCs distribute with a pro-lymphoid/erythroid bias with a shift toward myeloid output in adulthood. By mining transcriptomic data comparing juvenile and adult HSPCs and reconstructing coordinately activated gene regulatory networks, we uncover the Polycomb repressor complex 1 (PRC1) component Cbx2 as an effector of Lin28b/*let-7*'s control of hematopoietic maturation. We find that juvenile *Cbx2*$^{-/-}$ hematopoietic tissues show

*Correspondence: grant_rowe@dfci.harvard.edu.

AUTHOR CONTRIBUTIONS

Conceptualization, R.G.R.; methodology, R.G.R.; formal analysis, R.G.R., Q.Z., N.L., E.L.d.R., and M.K.; investigation, D.W., M.Y., E.M., T.L., E.L.d.R., and R.G.R.; resources, T.E.N.; data curation, R.G.R. and E.L.d.R.; writing – original draft, R.G.R.; writing – revising and editing, R.G.R.; Supervision, T.E.N., G.Q.D., and R.G.R.; Project administration, T.E.N., G.Q.D., and R.G.R.; Funding acquisition, G.Q.D. and R.G.R.

DECLARATION OF INTERESTS

G.Q.D. is a founder and shareholder of 28/7 Therapeutics.

SUPPLEMENTAL INFORMATION

Supplemental information can be found online at https://doi.org/10.1016/j.celrep.2022.110587.

impairment of B-lymphopoiesis, a precocious adult-like myeloid bias, and that Cbx2/PRC1 regulates developmental timing of expression of key hematopoietic transcription factors. These findings define a mechanism of regulation of HSPC output via chromatin modification as a function of age with potential impact on age-biased pediatric and adult blood disorders.

In brief

Wang et al. demonstrate that the Polycomb repressive complex 1 component Cbx2 functions downstream of the heterochronic Lin28b/*let-7* axis in hematopoietic stem and progenitor cells to choreograph definitive hematopoietic maturation.

Graphical Abstract

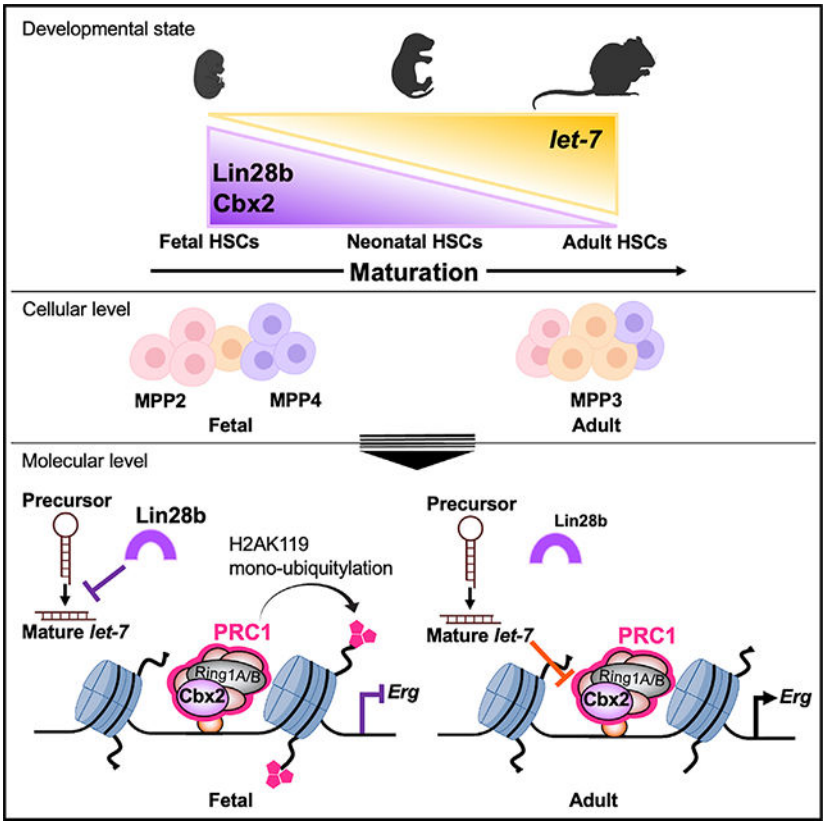

INTRODUCTION

Normal development and maturation require adaptation of stem cells to shifting physiologic priorities. During prenatal development, hematopoietic stem cells (HSCs) undergo rapid self-renewal to expand and establish the nascent definitive hematopoietic system within the fetal liver (FL) with an erythroid differentiation bias to support growth in the hypoxic uterus (Rebel et al., 1996a, 1996b; Rowe et al., 2016b). Following birth, juvenile hematopoiesis becomes lymphoid biased to establish and educate the adaptive immune system (MacKinney, 1978). In later life, hematopoiesis becomes myeloid biased, an effect that appears to be programmed at the level of HSCs and multipotent progenitors (MPPs)

(Pang et al., 2011; Young et al., 2016). These age-related changes in hematopoiesis are paralleled by age biases of blood diseases, including several distinct forms of leukemia and bone marrow (BM) failure disorders, illustrating the impact of normal development on disease manifestations (McKinney-Freeman et al., 2012; Rowe et al., 2019).

Recently and historically, much effort has focused on defining the molecular regulators of blood maturation from the fetus to the fully mature adult state. Hematopoietic maturation is associated with dramatic changes in gene expression and chromatin organization in hematopoietic stem and progenitor cells (HSPCs) (Bunis et al., 2021; Copley et al., 2013; Huang et al., 2016; Rowe et al., 2016b). As an example, the Polycomb repressor complex 2 (PRC2) component Ezh1 is downregulated during the developmental transition from primitive to definitive hematopoiesis to derepress transcriptional programs implementing definitive HSC traits (Vo et al., 2018). As a second example, during maturation of the definitive hematopoietic system, the transcriptional repressor BCL11A controls one of the most well-studied hematopoietic maturation processes, globin switching, by directly silencing human fetal globin (Basak et al., 2020). During definitive hematopoietic development, PRCs are variably required for many aspects of fetal and adult blood formation but the upstream molecular regulation of these heterochronic effects is undefined (Park et al., 2003; Xie et al., 2014).

The heterochronic RNA binding protein Lin28b is a key regulator of definitive hematopoietic maturation. Lin28b has been shown to regulate globin switching, self-renewal of HSCs, and both myeloid and lymphoid maturation via repression of the *let-7* family of microRNAs and modulation of their downstream targets, as well as through *let-7*-independent mechanisms (Basak et al., 2020; Copley et al., 2013; Rowe et al., 2016a, 2016b; Yuan et al., 2012). Although Lin28b directly and indirectly controls the translation of a multitude of RNAs, the specific mechanisms by which it exerts such profound effects on hematopoiesis have remained elusive. Here, we implicate the *let-7* target and PRC1 component Cbx2 in developmental maturation of HSPCs. We find that HSCs and MPPs redistribute and reprioritize their linage output during development and maturation, and that juvenile lymphoid- and erythroid-biased hematopoietic output requires Cbx2. Cbx2, via regulation of chromatin modifications by PRC1, modulates enhancers controlling master hematopoietic transcription factors for effective developmentally timed expression. These findings reveal how HSPCs mature over time and uncover a master axis required for effective hematopoietic maturation.

RESULTS

HSPCs undergo developmental maturation

To gain understanding of the developmental maturation of HSPCs, we profiled various populations of primitive HSCs and MPPs during maturation of the definitive hematopoietic system. We found that, within the Lineage$^-$ Sca-1$^+$ CD117$^+$ (LSK) fraction, lymphoid-biased MPP-4 declined progressively over time (Figures 1A–1C). In line with the shift away from erythroid toward myeloid output among progenitors during maturation from fetal to adult that we reported previously and confirmed here now, including neonates (Rowe et al., 2016b), we found that, at the MPP level, erythroid-biased MPP-2 diminished while

myeloid-biased MPP-3 increased with maturation (Figures 1A–1D and S1A). We did not observe significant differences in the quantity of phenotypic HSCs save for a short-term (ST)-HSC contraction with aging, consistent with prior reports (Figures 1A–1C) (Pang et al., 2011). The observed changes in MPP-4 paralleled the content of the peripheral blood counts, with neonates possessing higher absolute lymphocyte counts than adults, with a shift toward monocyte output occurring with aging (Figure 1E). We also observed increased mean corpuscular volume (MCV) in neonates relative to adults with an overall lower hemoglobin content (Figure 1E). These findings recapitulate known age-dependent changes in peripheral blood parameters described in humans (MacKinney, 1978; Saarinen and Siimes, 1978; van Gent et al., 2009).

To functionally validate these lineage priorities ingrained within LSKs, we isolated long-term HSCs (Lineage$^-$ CD117$^+$ Sca-1$^+$ CD127$^-$ CD48$^-$ CD150$^+$; LT-HSCs) from midgestation (embryonic week 14.5 [E14.5]) FL, newborn (postnatal day 0–1 [P0–1]) BM, or young adult (postnatal age 6–8 weeks) BM. transplanted them into lethally irradiated congenic adult recipients and monitored lineage output in the donor-derived fraction. We found that E14.5 FL and neonatal LT-HSCs showed significantly more B cell output at the 4-week time point compared with young adult LT-HSCs, which produced nearly only myeloid cells (Figures 1F and 1G). After 4 weeks, adult LT-HSCs produced progressively more B cells, while LT-HSCs of all ages begat T-cells with similar kinetics (Figures 1F and 1G). Notably, these differences were obscured when we transplanted whole hematopoietic tissue from each of these sources, suggesting that they are programmed at the level of early HSCs (Figure S1B and C).

HSPC distribution is controlled by the Lin28b/*let-7* axis

Lin28b is a well-established heterochronic factor regulating the timing of developmental events (Shyh-Chang and Daley, 2013). In the hematopoietic system, Lin28b is expressed in the fetal state where it regulates lymphoid differentiation, HSC self-renewal, platelet activation, and myeloid progenitor distributions, with its expression decreasing in HSCs with maturation; many of these effects are mediated by repression of the maturation of *let-7* microRNAs (Rowe et al., 2016a). We confirmed that *LIN28B* and several of its putative downstream effectors decrease with maturation in human and mouse HSPCs (e.g., *IGF2BP3*, *HMGA2*, and *IGF2BP1*; Figures 2A and S2A–S2D) (Beaudin et al., 2016; Cesana et al., 2018; Kugel et al., 2016). We also observed that the *LIN28B* promoter is developmentally regulated (Figure S2E) (Huang et al., 2016). We next examined the effect of ectopic activation of LIN28B within the adult BM on HSCs and MPPs. Here, we used a double transgenic system for activation of LIN28B in the upon doxycycline treatment for 2 weeks prior to transplantation—a duration effective to reprogram HSPC distributions —followed by transplantation of marrow and measurement of the HSPC compartment at 12 weeks to examine the output of long-term engrafting cells (Rowe et al., 2016b). At 12 weeks post transplantation, we found that LIN28B activation tended to diminish MPP-3, increased MPP-4, and diminished LT-HSCs consistent with partial implementation of a fetal HSC/MPP state (Figures 2B and 2C) (Young et al., 2021). Finally, we ectopically expressed a degradation-resistant form of *let-7g* in the adult marrow for 2 weeks prior to transplantation and constitutively post transplantation using a doxycycline-inducible

transgenic system, finding that this altered adult LSKs, with an increase in MPP-3 and diminishment of MPP-2 (Figures 2D and 2E) (Rowe et al., 2016b). However, we did not observe this shift in MPPs reflected in the peripheral blood, likely due to inhibitory effects of high LIN28B expression on lymphocyte effector differentiation (Table S1) (Rao et al., 2012). Together, these data demonstrate the Lin28b/*let-7* modulates the developmental state of HSCs and MPPs. These effects on HSCs and MPPs parallel effects on myeloerythroid progenitors, where Lin28b promotes an erythroid bias prenatally and *let-7* microRNAs drive a pro-myeloid distribution (Rowe et al., 2016b).

Cbx2 is a developmentally regulated Lin28b/*let-7* target in the hematopoietic system

Next, we endeavored to determine the downstream mediators of Lin28b′s effect on HSPC maturation. We used the CellNet algorithm to query 1,787 mouse gene regulatory subnetworks (GRSs) incorporating 717,140 genetic interactions using a published hematopoietic progenitor RNA-seq (RNA-seq) dataset (Cahan et al., 2014; Rowe et al., 2016b). This dataset includes common myeloid progenitors (CMPs) from E14.5 FL, WT adult BM, and adult BM ectopically expressing LIN28B (iLIN28B) to determine which GRSs are coordinately enriched in E14.5 FL and the FL-like maturation state implemented by ectopic LIN28B (Figure 3A) (Rowe et al., 2016b). We found 23 and 19 GRSs coordinately activated and repressed, respectively, in E14.5 FL and ectopic LIN28B marrow (Figure 3B). Focusing on GRSs active in hematopoietic tissues (blood subnetworks), we found three and five GRSs activated and repressed, respectively (Figure 3B). We next queried coordinately regulated GRSs for predicted *let-7* microRNA targets using Targetscan, which would be predicted to be increased in LIN28B-expressing cells (Agarwal et al., 2015). Using this approach, we identified the conserved *let-7* target *Cbx2* as enriched in E14.5 FL and iLIN28B adult CMPs compared with *Lin28b*$^{-/-}$ FL CMPs and WT adult CMPs (Figures 3C and 3D). Cbx2 was an appealing target, as regulation of a PRC1 component was an intriguing potential mechanism by which Lin28b and *let-7* microRNAs regulate HSPC maturation.

We found that *CBX2* expression was higher in human FL HSCs compared with adult HSCs (Figure 3E) (Cesana et al., 2018). By analyzing datasets comparing gene expression in murine fetal versus adult HSCs, we found that *Cbx2* transcripts were reproducibly higher in fetal cells (Figures 3F–3H) (Beaudin et al., 2016; Chen et al., 2019; Tober et al., 2018). However, we did not observe developmental regulation of the *CBX2* promoter, consistent with its regulation being post-transcriptional (Figure S2F) (Huang et al., 2016). Using human erythroid progenitor cells lines derived from neonatal (HUDEP-1) or adult (HUDEP-2) HSPCs, we found that CBX2 protein was higher in HUDEP-1 cells (Figures 3I and S3A) (Kurita et al., 2013).

We next sought to determine whether the Lin28b/*let-7* axis could control CBX2 in hematopoietic cells. We found that induction of LIN28B expression in adult mouse BM could increase Cbx2 protein (Figures 4A and S3B). Accordingly, doxycycline-induced activation of *let-7g* in the FL markedly decreased Cbx2 protein during juvenile hematopoiesis (Figures 4B–4C and S3C). Next, we used K562 cells, which possess the potential to express fetal hemoglobin as well as LIN28B, consistent with a fetal HSPC-like

state (Frigon et al., 1992; Ustianenko et al., 2018). First, we generated K562 cell lines with stable overexpression of *let-7g* or control cells bearing the empty vector (Figure 4D). We found that overexpression of *let-7g* diminished endogenous CBX2 protein with a concomitant decrease in LIN28B protein, another *let-7* target (Figures 4E and S3D). Next, we introduced a *let-7* sponge construct into K562 or HUDEP-2 cells (Kumar et al., 2008), which specifically sequesters mature *let-7* species (Figure 4F). Cells bearing this sponge showed increased CBX2 protein (Figures 4G–4H and S3E–S3F). Together, these findings indicate that the Lin28b/*let-7* axis controls CBX2 protein levels and suggest that CBX2 is a heterochronic regulator of hematopoiesis.

Cbx2 regulates juvenile hematopoietic output

Cbx2 regulates lymphoid proliferation and can perturb HSPCs upon overexpression, but its developmental stage-specific functions have not been investigated (Core et al., 2004; van den Boom et al., 2013). *Cbx2*-null mice develop skeletal anomalies and sex reversal, and typically die perinatally (Core et al., 1997). We therefore generated $Cbx2^{-/-}$ embryos and examined definitive FL hematopoiesis. Compared with $Cbx2^{+/+}$ and $Cbx2^{+/-}$ littermates, we observed significant diminishment of ST-HSCs and a trend toward diminished MPP-3 in $Cbx2^{-/-}$ FLs (Figure S4A–S4B). We did not observe significant differences in MPP-2, MPP-3, or MPP-4 at this time point (Figure S4A–S4B). However, we observed remodeling of myeloerythroid progenitors away from a fetal erythroid-dominant distribution and toward an adult-like myeloid predominance, consistent with precocious maturation as seen previously in FLs ectopically expressing *let-7g* (Figures 5A and 5B) (Rowe et al., 2016b). Consistent with this observation, we also observed a decrease in the master erythroid transcription factors *Gata1* and *Klf1* in $Cbx2^{-/-}$ neonatal BM and loss of a heme synthesis signature (Figures 5C and 5D) (Katoh-Fukui et al., 2019).

We next examined mature blood cell output. We first asked whether *Cbx2* regulates the youthful wave of lymphopoiesis. We found that the $Cbx2^{-/-}$ neonatal spleen was deficient in B cells (Figures 5E and 5F). $Cbx2^{-/-}$ B cells did not undergo precocious maturation from a fetal B-1a to a mature adult B-2 state, but rather showed impaired maturation (Figure S4C–S4D). B cells were undergoing apoptosis, likely contributing to the impaired maturation (Figure 5G). RNA-seq analysis revealed a decrease in transcripts encoding key B cell factors including *Pax5* in $Cbx2^{-/-}$ marrow with a relative gain of myeloid genes, including the master myeloid transcription factor *Spi1*/*Pu.1* and signatures associated with inflammatory responses (Figures 5H and 5I) (Katoh-Fukui et al., 2019).

We next directly examined the functional role of Cbx2 in governing HSPC differentiation. First, we transplanted $Cbx2^{-/-}$ MPP-4 isolated from E14.5 FL, which resulted in a diminishment of donor-derived B-lymphoid output compared with littermate $Cbx2^{+/+}$ FL MPP-4 (Figures 6A and 6B). Conversely, activation of Cbx2 in adult HSPCs, where it would be otherwise developmentally downregulated, resulted in skewing of cell output toward the erythroid lineage within GEMM (granulocyte, erythrocyte, monocyte/macrophage) colonies, consistent with a fetal-like phenotype (Figure 6C) (Rowe et al., 2016b). Finally, we turned to the zebrafish system, where we found that morpholino-mediated knockdown of *cbx2* in the developing embryo resulted in diminishment of *rag2:gfp*$^{+}$ lymphocytes in the thymus by

96 h post fertilization with a concomitant gain of *mpo:gfp*$^{+}$ myeloid cells in the embryo, recapitulating the phenotype observed in mice (Figures 6D–6G). Together, these results indicate that *Cbx2* regulates developmental age-specific hematopoiesis.

Cbx2 controls PRC1 activity in fetal HSPCs

To understand the role of Cbx2/PRC1 in juvenile hematopoiesis, we performed CUT&RUN for histone H2A lysine 119 monoubiquitinylation (H2AK119Ub), the hallmark of gene silencing by PRC1 required for maintenance of repression of target loci (Skene and Henikoff, 2017; Tamburri et al., 2020). First, we performed H2AK119Ub CUT&RUN using neonatal HUDEP-1 cells. We observed that H2AK119Ub distributed throughout gene bodies relative to histone H3 lysine 4 trimethylation (H3K4me3), which was localized to promoters as expected (Figure S5A). In these neonatal cells, we observed H2AK119Ub binding to the pro-myeloid transcription factors *GFI1* and *SPI1*, both of which showed higher levels of the activating histone mark histone H3 lysine 27 acetylation (H3K27Ac) in human adult relative to fetal HSPCs (Figure S5B).

To determine the functional role played by Cbx2 in developmental control of PRC1, we next isolated E14.5 FL HSPCs from *Cbx2*$^{-/-}$ embryos or *Cbx2*$^{+/+}$ littermate controls for CUT&RUN analysis. Here, we did not observe global disruption of H2AK119Ub localization in *Cbx2*$^{-/-}$ cells (Figure 7A). We identified several H2AK119Ub peaks significantly gained or lost in *Cbx2*$^{-/-}$ cells relative to controls using the MACS2 algorithm, with many peaks being intronic or intergenic, raising the possibility of regulation of enhancer elements (Figure 7B) (Feng et al., 2012). Gene ontology analysis of differential peaks (lost or gained) revealed enrichment of several terms related to hematopoiesis, particularly terms related to adaptive immunity (Figures 7C and S5C). Motif analysis of peaks diminished in *Cbx2*$^{-/-}$ HSPCs identified binding motifs for hematopoietic transcription factors (Figure 7D).

We next focused on peaks lost in *Cbx2*$^{-/-}$ HSPCs as potential PRC1 targets directly dependent on Cbx2. Notably, we did not observe differences in H2AK119 monoubiquitylation at the *Hoxa* or *Hoxb* clusters (Figure S5D–S5E). However, we observed differential H2AK119Ub abundance associated with a 1.4 kilobase (kb) intronic sequence within the *Erg* gene located 52 kb upstream of the transcriptional start site of the short Erg isoform, with this peak significantly different between *Cbx2*$^{+/+}$ and *Cbx2*$^{-/-}$ cells using MACS2 (Figure 7E) (Feng et al., 2012). This was of interest given the central role of Erg in HSPC self-renewal and differentiation (Knudsen et al., 2015; Taoudi et al., 2011). Analysis of H3K4me3 revealed that the promoter of the short *Erg* isoform was active, consistent with predominant utilization of this isoform in FL HSPCs (Figure 7E). We found several consensus binding sequences for CEBP, ETV6, and SPIB transcription factors within this interval, suggestive of enhancer activity (Figure 7F). We cloned a fragment of this candidate enhancer, finding that it strongly enhanced detectable basal transcription from a minimal promoter (Figure 7G). Supportive of its developmental regulation by Cbx2, *ERG*/*Erg* is expressed at higher levels in adult BM versus FL human and mouse HSPCs, *Erg* is increased in *Cbx2*$^{-/-}$ compared with *Cbx2*$^{+/+}$ neonatal BM, and the human *ERG* locus showed differential H3K27Ac in adult and FL HSPCs at apparent developmentally regulated

candidate human enhancer sequences associated with H2AK119Ub, and age-dependent changes in H3K27Ac in mouse HSPCs were observed (Chen et al., 2019; Huang et al., 2016; Katoh-Fukui et al., 2019; Tober et al., 2018) (Figures 7H and S6A–S6C). We confirmed that *Erg* expression is increased in perinatal spleens of $Cbx2^{-/-}$ mice compared with $Cbx2^{+/+}$ littermates (Figure 7I). Ectopic expression of Cbx2 resulted in repression of SPI1 protein levels and repressed *SPI1*, *ERG*, and *GFI1* transcripts (Figures 7J–7K and S6D). Taken together, these data support Cbx2/CBX2-mediated developmental regulation of *Erg*/*ERG* and other master hematopoietic transcription factors. Our results describe a mechanism by which Cbx2, via control of PRC1, regulates hematopoietic maturation (Carmichael et al., 2012; Tsuzuki et al., 2011).

DISCUSSION

Here, we find that definitive HSPCs undergo stereotypical remodeling during development and maturation from the fetus to the neonate and into young adulthood. We observed that HSCs and MPPs redistribute to reflect age-specific patterns of cell output, from juvenile erythroid- and lymphoid-biased output to mature myeloid predominance, demonstrating that age-associated lineage biases are ingrained early in hematopoietic differentiation. These results extend prior work on postnatal remodeling of the HSC/MPP compartment during aging from young to older adulthood by showing that the aging is preceded by a scripted process of maturation (Young et al., 2016).

The Lin28b/*let-7* axis is the most thoroughly investigated regulator of age-specific hematopoiesis (Copley et al., 2013; Rowe et al., 2016a, 2016b; Yuan et al., 2012). Lin28 paralogs are highly conserved heterochronic factors that control the schedule of developmental events in several species (Kiontke et al., 2019; Moss et al., 1997). Lin28b exerts wide-ranging effects in HSPCs, with its activity sufficient to impart juvenile hematopoiesis in adult cells either via inhibition of *let-7* microRNA stability or by directly regulating translation of specific mRNAs (Basak et al., 2020; Lee et al., 2013; Rowe et al., 2016b). Lin28b is downregulated during progression of development and maturation, releasing *let-7* microRNAs to implement adult hematopoiesis (Rowe et al., 2016b). As an oncofetal factor, Lin28 proteins have been implicated in the pathobiology of hematologic malignancies, suggesting that Lin28b might recruit fetal-specific HSPC traits in leukemia (Emmrich et al., 2014; Helsmoortel et al., 2016; Manier et al., 2017; Rao et al., 2012).

Here, we find that lymphoid-biased MPP-4 diminish with maturation, and that this process is controlled by Lin28b. Lin28b acts as a heterochronic regulator of lymphopoiesis, where its ectopic expression in mature adult HSCs can induce fetal-like lymphopoiesis characterized by γδ-T cell, B-1a, and marginal zone B cell production (Yuan et al., 2012). Subsequent studies have shown that the transcription factor Arid3a is expressed in fetal hematopoiesis and is a target of *let-7*; ectopic Arid3a can reprogram adult pro-B cells to produce fetal B-1 cells (Zhou et al., 2015). Lin28b cooperates with Igf2bp3 to stabilize both Pax5 and Arid3a to implement fetal B-lymphopoiesis (Wang et al., 2019). Downstream of differentiation, Lin28b functions in neonatal B cell positive selection (Vanhee et al., 2019). Our results add to these observations in that we find that not only does Lin28 implement juvenile B-

lymphoid differentiation states but it also controls juvenile lymphoid-biased hematopoiesis at the level of HSCs/MPPs, at least in part through Cbx2/PRC1.

Fetal and neonatal hematopoiesis are associated with the production of transient innate-like lymphocyte states, followed by a quantitative burst of lymphoid output presumably to establish innate immunity upon birth. It is well known that the lymphocyte count decreases with aging from childhood to adulthood (Falcao, 1980; MacKinney, 1978). The human thymus forms and is populated by developing lymphocytes undergoing selection in midgestation but begins the process of involution in the first decade of life (Farley et al., 2013; Palmer et al., 2018). It has been hypothesized that dysregulation of this crucial period of postnatal immune education contributes to the risk of developing childhood lymphoblastic leukemia, illustrative of the unique properties of this developmental window (Greaves, 2018). Our work demonstrates that timing of this juvenile lymphopoietic wave is programmed into HSCs/MPPs by the Lin28b/*let-7*/Cbx2 axis.

Through analysis of collections of GRSs cross-referenced with *let-7* targets, we identified Cbx2 as a regulator of hematopoietic maturation. Recently, a Lin28a-*let-7*-Cbx2 axis was suggested to control skeletal formation via control of *Hox* gene expression (Sato et al., 2020). Although many *Hox* genes regulate the function of normal and malignant HSPCs, we did not observe developmental regulation of *Hox* loci in HSCs and MPPs (Smith et al., 2011; Yu et al., 2014). We demonstrate alterations of *Cbx2* gene expression with age at the transcript level in HSC/MPPs and at the protein level in HSPCs lines derived from newborn or mature donors in response to modulation of Lin28b/*let-7* (Kurita et al., 2013). In addition to its role in promoting juvenile lymphoid output, the Lin28b/*let-7* axis fine-tunes myeloerythroid output for age-appropriate physiology (Rowe et al., 2016b). We find that $Cbx2^{-/-}$ mice show a precocious adult-like myeloid-biased progenitor distribution, consistent with its role as an effector of Lin28b′s control over hematopoietic maturation. Our data suggest that this is due at least in part to Cbx2's ability to modulate the expression of key HSPC transcription factors that likely serve to program lineage preferences within HSCs and MPPs. These data define Cbx2 as a heterochronic factor within the hematopoietic system that participates in defining age-specific lineage outputs at the level of HSPCs.

Prior to our study, Cbx2 had been implicated in both hematopoiesis and lymphopoiesis. The initial characterization of $Cbx2^{-/-}$ mice reported that these mice showed involution of the thymus and small splenic size at 3–4 weeks of age, with impaired proliferation of splenocytes (Core et al., 1997). Altered B and T cell differentiation was subsequently reported in $Cbx2^{-/-}$ mice (Core et al., 2004). These findings further support a crucial role for Cbx2 in the juvenile lymphoid expansion. Knockdown of *CBX2* in human umbilical cord blood $CD34^{+}$ cells resulted in impaired HSPC self-renewal and skewing away from erythroid and toward myeloid output, paralleling our findings (van den Boom et al., 2013). Relative to lineage-restricted progenitors, Cbx2 is most enriched in HSCs and B- and T-lymphocytes, and its overexpression inhibits clonogenesis and repopulation in transplantation assays, suggesting that its activity must be finely balanced (Klauke et al., 2013). While prior studies have defined roles for Cbx2 in HSC and MPP function, our work places the hematopoietic functions of Cbx2 within the context of normal development,

maturation, and aging, and places Cbx2 as an important downstream regulator of the heterochronic Lin28/*let-7* pathway.

We find that Cbx2 regulates age-dependent expression of *Erg* during hematopoietic maturation. We focused on this differentially regulated enhancer given the central role of *Erg* in regulation of HSPC maintenance and differentiation (Knudsen et al., 2015; Taoudi et al., 2011). Hematopoietic transcription factors collaborate in gene regulatory networks to control central properties of HSPCs (Khajuria et al., 2018). Given the dependency of HSCs on Erg for their maintenance, we would not expect *Erg* to be markedly silenced in the adult or fetal states; rather, alterations in expression of such master transcription factors likely fine-tune the balance of HSPC maintenance and differentiation to maintain age-appropriate homeostasis.

It is becoming increasingly apparent that PRCs play important roles in the timing of hematopoietic development and maturation phenotypes and are also dysregulated in blood malignancies. PRCs likely play key roles in the regulation of stage-specific enhancer usage (Huang et al., 2016). Loss of *Ezh1* in the mouse embryo results in precocious unlocking of hallmarks of definitive HSCs in primitive hematopoietic progenitors (Vo et al., 2018). Deletion of *Ezh2* in FL HSCs causes hematopoietic failure associated with reduction in H3K27me3, while its loss in adult BM HSCs results in a much less severe phenotype, likely due to programmed upregulation of Ezh1, which can compensate for Ezh2 loss (Mochizuki-Kashio et al., 2011). Effects of *Ezh2* deficiency on hematopoiesis in the FL appear to be due to both extrinsic and intrinsic effects (Neo et al., 2018). Genetic ablation of *Eed*, which disrupts both Ezh1- and Ezh2-containing PRC2 complexes, is tolerated by FL hematopoiesis but depletes adult BM HSCs (Xie et al., 2014). Deficiency of the PRC1 component *Bmi1* is tolerated by FL HSCs at steady state, but the BM of adult mice is progressively depleted of HSCs, apparently due to dysregulated self-renewal (Park et al., 2003). Here, we define how the Lin28b/*let-7* axis—a master regulator of hematopoietic maturation—integrates with PRC1 via Cbx2 to control age-specific hematopoietic output through regulation of chromatin modifications, explaining how Lin28b exerts such broad effects within the hematopoietic system as a master regulator of HSPC developmental maturation. Loss of Cbx2 dysregulates PRC1 broadly, as shown by both loss and gain of H2AK119Ub peaks throughout the genome. Investigation of how loss of Cbx2 or other Cbx proteins perturbs PRC1 homeostasis remains an important open question. These findings deepen understanding of how the hematopoietic system changes with age and have potential translational impact on understanding the mechanisms by which blood disorders are biased toward particular ages.

Limitations of the study

Although we combined human, mouse, and zebrafish model systems, the functional role of the proposed Lin28b-*let-7*-Cbx2-Erg axis in human hematopoietic maturation must be demonstrated in future study. This is of particular importance to gain understanding of the role of this heterochronic axis in age-skewed blood diseases such as leukemia. Although we focused on the role of this axis in regulating lineage biases in HSPCs, its function in

age-related differences in HSC self-renewal has not yet been addressed (Copley et al., 2013). These open questions not addressed here form the basis for future study.

STAR★METHODS

RESOURCE AVAILABILITY

Lead contact—Further information and requests for resources and reagents should be directed to and will be fulfilled by the lead contact, Grant Rowe (grant_rowe@dfci.harvard.edu).

Materials availability—Plasmids generated in this study will be deposited to Addgene prior to the date of publication or are available upon request from the Lead Contact.

Data availability

- Next generation sequencing CUT&RUN data (raw mouse and process human data) have been deposited in Gene Expression Omnibus and are publicly available at the date of publication. Raw CUT&RUN data derived from human samples have been deposited in the NIH Database of Genotypes and Phenotypes. Prior to publication, the authors officially requested that the raw datasets reported in this paper be made publicly available. To request access, contact the Lead Contact. These accession numbers are listed in the key resources table.
- This paper does not report original code.
- Any additional information required to reanalyze the data reported in this paper is available from the Lead Contact upon request.

EXPERIMENTAL MODEL AND SUBJECT DETAILS

Animals were utilized in accordance with approvals from the Boston Children's Hospital Institutional Animal Care and Use Committees.

Mice and transplantation studies—C57BL/6J (CD45.2) and SJL (CD45.1) mice were from Jackson Laboratory. Timed pregnancies were used to isolate FL cells on post-coital day 14.5 and neonatal day 0–1. 6–8-week-old mice were used for comparison. *Cbx2*$^{-/-}$ mice (M33-) were from Jackson Laboratory (stock 006,002) (Core et al., 1997). For HSC transplantations, mice were conditioned with a lethal dose of 975 rad prior to injection of CD45.2 donor cells via the tail vein into CD45.1 recipients. For progenitor transplants, mice were conditioned with sublethal 675 rad prior to injection. For iLIN28B and i*let-7g* transplantation, double transgenic mice were induced with doxycycline drinking water (1 g/L) for two weeks prior to transplantation as this seemed to be the maximal tolerated duration of global LIN28B induction (Rowe et al., 2016b). Since sex of neonatal and fetal mice is not readily discerned, approximately equal sex distributions are assumed in experiments using these animals, and adult cohorts to which they compared contained approximately equal male and female mice.

Zebrafish use and analysis—Validated splice-blocking morpholino oligonucleotides (GeneTools) targeting *cbx2* [5′-TAGTTTCCTGAGAGAGGAACACAAA-3′] were injected (1–2 nL of 50 μM MO) at the 1-cell stage as previously detailed (Cortes et al., 2016; Huang et al., 2013). Flow cytometry was performed using transgenic *Tg*(*rag2:GFP*) or *Tg*(*mpo:GFP*) embryos at 96 hpf (Renshaw et al., 2006; Traver et al., 2003). Embryos (pools of 5 embryos per sample, 8 replicates) were dissociated and analyzed following staining with SYTOX Red viability stain (ThermoFisher). Both male and female fish were included in the analysis with no exclusion of either sex.

METHOD DETAILS

Cell culture—HUDEP-1 (RRID:CVCL_VI05) and HUDEP-2 (RRID:CVCL_VI06) cells were obtained from RIKEN and maintained in SFEM (Stem Cell Technologies) supplemented with 50 ng/mL SCF (R and D Systems), 3 units/ml recombinant erythropoietin (PeproTech), 1 μg/mL doxycycline, and 1 μM dexamethasone. K562 cells (RRID:CVCL_0004) were maintained in IMDM with 10% fetal calf serum.

Flow cytometry—The following antibodies were used (all from BioLegend): CD3 (clone 17A2), Ter119 (TER-119), Gr-1 (RB6–8C5), B220 (RA3–6B2) conjugated to Pacific Blue, CD117 APC-Cy7 (2B8), Sca-1 PE-Cy7 (D7), Flk2 PE (A2F10), CD48 FITC (HM48–1), CD150 APC (TC15–12F12.2), B220 PE-Cy7 (RA3–6B2), Mac-1 PE-Cy5 (M1/70), CD3 PE (17A2), Ter119 APC-Cy7 (TER-119), CD45.2 FITC (104), CD45.1 APC-Cy7 (A20), CD16/32 PerCP-Cy5.5 (93), CD5 APC-Cy7 (53–7.3). CD19 PE (eBio1D3) and CD34 FITC (RAM34) were from eBioscience. Cells were labeled with SYTOX Blue viability stain (Thermo). Data were acquired on LSRII or LSR Fortessa instruments (BD Biosciences). APC-annexin V was from BioLegend.

Purification of cells—For LT-HSC or MPP-4 sorting, bone marrow and FL cells were positively selected by CD117 MicroBeads (Miltenyi Biotec). Enriched cells were stained with antibodies against Ter119, B220, CD3, Gr1, c-Kit, Sca-1, Flk2, CD150, and CD48. Then we added SYTOX Blue to exclude dead cells and sorted $Lin^{-}c\text{-}kit^{+}Sca\text{-}1^{+}Flk2^{+}$ for MPP4 and $Lin^{-}c\text{-}kit^{+}Sca\text{-}1^{+}Flk2^{-}CD48^{-}CD150^{+}$ for LT-HSC.

Gene regulatory subnetwork analysis—Annotated gene regulatory subnetworks generated by the CellNet algorithm (Cahan et al., 2014) were used in gene set enrichment analysis against preranked lists generated from RNA-sequencing-based comparison of WT fetal liver CMPs, WT young adult CMPs, or young adult CMPs ectopically expressing LIN28B (Rowe et al., 2016b). Subnetworks with positive enrichment scores were examined for predicted *let-7* target sites using the Targetscan algorithm (Agarwal et al., 2015).

Western blotting—The following antibodies were used: CBX2 (Abcam 80,044 or Bethyl A302–524A), LIN28B (Cell Signaling Technologies 11,965, clone D4H1), SPI1/PU.1 (Cell Signaling Technologies 2258), H2AK119Ub (Cell Signaling Technologies 8240) and β-actin (Cell Signaling Technologies 4970). Western blots were quantified with ImageJ software.

Quantitative RT-PCR—RNA was purified with TRIzol™ Reagent (Thermo) and synthesized complementary DNA (cDNA) by SuperScript II Reverse Transcriptase (Thermo). The cDNA samples were amplified using Power SYBR™ Green PCR Master Mix (Thermo) and the QuantStudio™ 7 Flex Real-Time PCR System (Applied Biosystems). Primer assays for microRNA species were purchased from Qiagen. Human *CBX2* primers were: F: 5′-GACAGAACCCGTCAGTGTCC-3′, R: 5′-GGCTTCAGTAATGCCTCAGGT-3’. Human *GAPDH* primers were F: 5′-GTCTCCTCTGACTTCAACAGCG-3′, R: 5′-ACCACCCTGTTGCTGTAGCCAA-3′. Human *GFI1* primers were: F: 5′-GAGCCTGGAGCAGCACAAAG-3′, R: 5′-GTGGATGACCTCTTGAAGCTCTTC-3′. Human *SPI1* primers were: F: 5′-GACACGGATCTATACCAACGCC-3′, R: 5′-CCGTGAAGTTGTTCTCGGCGAA-3′. Human *ERG* primers were: F: 5’-GGACAGACTTCCAAGATGAGCC-3’, R: 5′-CCACACTGCATTCATCAGGAGAG-3′. Mouse β-actin primers were: F: 5′-ACGAGGCCCAGAGCAAGAGAGG-3′ and R: 5’-ACGCACCGATCCACACAGAGTA-3′. Mouse *Erg* primers were: F: 5’-GAGTGGGCGGTGAAAGAATA-3′ and R: 5’-TCAACGTCATCGGAAGTCAG-3′. For let-7g detection, we used miScriptII kit (QIAGEN).

Molecular cloning—pMSCV-neo let-7g was a gift from Tyler Jacks (Addgene plasmid # 14,784) (Kumar et al., 2007). pMSCV-puro let-7 sponge was a gift from Phil Sharp (Addgene plasmid # 29,766) (Kumar et al., 2008). For ectopic Cbx2 expression, the mouse Cbx2 open reading frame cDNA (Genecopoieia) was cloned into pCW57.1 (gift from David Root; Addgene plasmid # 41,393). To generate the *Erg* reporter construct, 162-mer double-stranded oligonucleotides containing Erg enhancer sequences were inserted into the pNL3.1 Vector (#N1031, Promega, USA) to establish the pNL3.1-Erg vector.

Stable cell lines—K562 (ATCC) cells were transfected with the indicated constructs using the Lipofectamine LTX reagent following standard protocols (Thermo). 24 h following transfection, cells were changed to fresh medium. 48 h post-transfection, stable transfected cells were selected either with puromycin (2 μg/mL) or G418 (1 mg/mL) in parallel with untransfected cells. When all untransfected cells were dead, stable cell lines were used for the indicated experiments at two weeks following selection. HUDEP-1 and HUDEP-2 cells were transduced with the indicated constructs using retrovirus packaged in HEK-293T cells (ATCC) and selected with puromycin (0.5 μg/mL)

Reporter assays—K562 cells were co-transfected with pGL4.50 vector (Promega, USA) and pNL3.1 or pNL3.1-Erg. Twenty-four hours after transfection, cells were analyzed for luciferase activity by Nano-Glo® Dual-Luciferase® Reporter Assay System (Promega, USA) and Synergy™ NEO (BioTek). The normalized signal for firefly luciferase activity (NanoLuc luciferase activity/firefly luciferase activity) was calculated and normalized to the signal of non-transfected wells.

CUT&RUN and data analysis—CUT&RUN was done according to the manufacturer’s protocol (EpiCypher). We used 200,000–500,000 flow sorted mouse Lin^- $Sca\text{-}1^+$ $c\text{-}kit^+$ HSPCs or K562 or HUDEP-1 cells for each experiment. Raw data were processed

using FastQC and CUT&RUNTools and mapped to mm10 (Zhu et al., 2019). Parameters of individual software called by CUT&RUNTools, including Bowtie2, Trimmomatic, Picard (http://broadinstitute.github.io/picard/), Samtools were left unchanged. *E. coli* spike-in DNA was used for normalization. We mapped the sequencing reads to *E. coli* genome using Bowtie2 (–end-to-end –very-sensitive –no-overlap –no-dovetail –no-mixed –no-discordant) and calculated the "spike_in_ratio" in each sample as "Ecoli_reads/Total_reads". The bigwig tracks were generated using bamCoverage from deeptools package with "scale_factor" calculated as 1/(spike_in_ratio * cell_number_factor), where "cell_number_factor" to balance signal based on cell input. For human HUDEP-1 and K562 cells, analysis was performed on the Basepair platform with alignment done with Bowtie2 (basepairtech.com). Differential peak calling was completed with MACS2 and motif analysis was done with Hypergeometric Optimization of Motif EnRichment (HOMER) (Feng et al., 2012).

QUANTIFICATION AND STATISTICAL ANALYSIS

Statistical analysis was performed in Prism and Excel. The statistical details of individual experiments can be found in the figure legends including the statistical tests used, value of n, what n represents, number of experiments, and definition of center with precision measures.

Supplementary Material

Refer to Web version on PubMed Central for supplementary material.

ACKNOWLEDGMENTS

This work was supported by the National Institute of Diabetes and Digestive and Kidney Diseases (K08 DK114527-01 to R.G.R.), the National Heart, Lung, and Blood Institute (U01 HL134812 to G.Q.D.), and the Coordination for Improvement of Higher Education Personnel (CAPES/Brazil to E.L.d.R.). The graphical abstract was created with Biorender.com.

REFERENCES

Agarwal V, Bell GW, Nam JW, and Bartel DP (2015). Predicting effective microRNA target sites in mammalian mRNAs. Elife 4, e05005.

Basak A, Munschauer M, Lareau CA, Montbleau KE, Ulirsch JC, Hartigan CR, Schenone M, Lian J, Wang Y, Huang Y, et al. (2020). Control of human hemoglobin switching by LIN28B-mediated regulation of BCL11A translation. Nat. Genet. 52, 138–145. [PubMed: 31959994]

Beaudin AE, Boyer SW, Perez-Cunningham J, Hernandez GE, Derderian SC, Jujjavarapu C, Aaserude E, MacKenzie T, and Forsberg EC (2016). A transient developmental hematopoietic stem cell gives rise to innate-like B and T cells. Cell Stem Cell 19, 768–783. [PubMed: 27666010]

Bunis DG, Bronevetsky Y, Krow-Lucal E, Bhakta NR, Kim CC, Nerella S, Jones N, Mendoza VF, Bryson YJ, Gern JE, et al. (2021). Single-cell mapping of progressive fetal-to-adult transition in human naive T cells. Cell Rep. 34, 108573. [PubMed: 33406429]

Cahan P, Li H, Morris SA, Lummertz da Rocha E, Daley GQ, and Collins JJ (2014). CellNet: network biology applied to stem cell engineering. Cell 158, 903–915. [PubMed: 25126793]

Carmichael CL, Metcalf D, Henley KJ, Kruse EA, Di Rago L, Mifsud S, Alexander WS, and Kile BT (2012). Hematopoietic overexpression of the transcription factor erg induces lymphoid and erythro-megakaryocytic leukemia. Proc. Natl. Acad. Sci. U S A. 109, 15437–15442. [PubMed: 22936051]

Cesana M, Guo MH, Cacchiarelli D, Wahlster L, Barragan J, Doulatov S, Vo LT, Salvatori B, Trapnell C, Clement K, et al. (2018). A CLK3-HMGA2 alternative splicing axis impacts human hematopoietic stem cell molecular identity throughout development. Cell Stem Cell 22, 575–588.e577. [PubMed: 29625070]

Chen C, Yu W, Tober J, Gao P, He B, Lee K, Trieu T, Blobel GA, Speck NA, and Tan K (2019). Spatial genome re-organization between fetal and adult hematopoietic stem cells. Cell Rep 29, 4200–4211.e4207. [PubMed: 31851943]

Copley MR, Babovic S, Benz C, Knapp DJ, Beer PA, Kent DG, Wohrer S, Treloar DQ, Day C, Rowe K, et al. (2013). The Lin28b-let-7-Hmga2 axis determines the higher self-renewal potential of fetal haematopoietic stem cells. Nat. Cell Biol. 15, 916–925. [PubMed: 23811688]

Core N, Bel S, Gaunt SJ, Aurrand-Lions M, Pearce J, Fisher A, and Djabali M (1997). Altered cellular proliferation and mesoderm patterning in polycomb-M33-deficient mice. Development 124, 721–729. [PubMed: 9043087]

Core N, Joly F, Boned A, and Djabali M (2004). Disruption of E2F signaling suppresses the INK4a-induced proliferative defect in M33-deficient mice. Oncogene 23, 7660–7668. [PubMed: 15377996]

Cortes M, Chen MJ, Stachura DL, Liu SY, Kwan W, Wright F, Vo LT, Theodore LN, Esain V, Frost IM, et al. (2016). Developmental vitamin D availability impacts hematopoietic stem cell production. Cell Rep 17, 458–468. [PubMed: 27705794]

Emmrich S, Katsman-Kuipers JE, Henke K, Khatib ME, Jammal R, Engeland F, Dasci F, Zwaan CM, den Boer ML, Verboon L, et al. (2014). miR-9 is a tumor suppressor in pediatric AML with t(8;21). Leukemia 28, 1022–1032. [PubMed: 24270738]

Falcao RP (1980). Human blood lymphocyte subpopulations from birth to eight years. Clin. Exp. Immunol. 39, 203–207. [PubMed: 6966987]

Farley AM, Morris LX, Vroegindeweij E, Depreter ML, Vaidya H, Stenhouse FH, Tomlinson SR, Anderson RA, Cupedo T, Cornelissen JJ, et al. (2013). Dynamics of thymus organogenesis and colonization in early human development. Development 140, 2015–2026. [PubMed: 23571219]

Feng J, Liu T, Qin B, Zhang Y, and Liu XS (2012). Identifying ChIP-seq enrichment using MACS. Nat. Protoc. 7, 1728–1740. [PubMed: 22936215]

Frigon NL Jr., Shao L, Young AL, Maderazo L, and Yu J (1992). Regulation of globin gene expression in human K562 cells by recombinant activin A. Blood 79, 765–772. [PubMed: 1732015]

Greaves M (2018). A causal mechanism for childhood acute lymphoblastic leukaemia. Nat. Rev. Cancer 18, 471–484. [PubMed: 29784935]

Helsmoortel HH, De Moerloose B, Pieters T, Ghazavi F, Bresolin S, Cave H, de Vries A, de Haas V, Flotho C, Labarque V, et al. (2016). LIN28B is over-expressed in specific subtypes of pediatric leukemia and regulates lncRNA H19. Haematologica 101, e240–244. [PubMed: 26969084]

Huang HT, Kathrein KL, Barton A, Gitlin Z, Huang YH, Ward TP, Hofmann O, Dibiase A, Song A, Tyekucheva S, et al. (2013). A network of epigenetic regulators guides developmental haematopoiesis in vivo. Nat. Cell Biol 15, 1516–1525. [PubMed: 24240475]

Huang J, Liu X, Li D, Shao Z, Cao H, Zhang Y, Trompouki E, Bowman TV, Zon LI, Yuan GC, et al. (2016). Dynamic control of enhancer repertoires drives lineage and stage-specific transcription during hematopoiesis. Dev. Cell 36, 9–23. [PubMed: 26766440]

Katoh-Fukui Y, Baba T, Sato T, Otake H, Nagakui-Noguchi Y, Shindo M, Suyama M, Ohkawa Y, Tsumura H, Morohashi KI, et al. (2019). Mouse polycomb group gene Cbx2 promotes osteoblastic but suppresses adipogenic differentiation in postnatal long bones. Bone 120, 219–231. [PubMed: 30389610]

Khajuria RK, Munschauer M, Ulirsch JC, Fiorini C, Ludwig LS, McFarland SK, Abdulhay NJ, Specht H, Keshishian H, Mani DR, et al. (2018). Ribosome levels selectively regulate translation and lineage commitment in human hematopoiesis. Cell 173, 90–103.e119. [PubMed: 29551269]

Kiontke KC, Herrera RA, Vuong E, Luo J, Schwarz EM, Fitch DHA, and Portman DS (2019). The long non-coding RNA lep-5 promotes the juvenile-to-adult transition by destabilizing LIN-28. Dev. Cell 49, 542–555.e549. [PubMed: 30956008]

Klauke K, Radulovic V, Broekhuis M, Weersing E, Zwart E, Olthof S, Ritsema M, Bruggeman S, Wu X, Helin K, et al. (2013). Polycomb Cbx family members mediate the balance between

haematopoietic stem cell self-renewal and differentiation. Nat. Cell Biol 15, 353–362. [PubMed: 23502315]

Knudsen KJ, Rehn M, Hasemann MS, Rapin N, Bagger FO, Ohlsson E, Willer A, Frank AK, Søndergaard E, Jendholm J, et al. (2015). ERG promotes the maintenance of hematopoietic stem cells by restricting their differentiation. Genes Dev. 29, 1915–1929. [PubMed: 26385962]

Kugel S, Sebastian C, Fitamant J, Ross KN, Saha SK, Jain E, Gladden A, Arora KS, Kato Y, Rivera MN, et al. (2016). SIRT6 suppresses pancreatic cancer through control of Lin28b. Cell 165, 1401–1415. [PubMed: 27180906]

Kumar MS, Erkeland SJ, Pester RE, Chen CY, Ebert MS, Sharp PA, and Jacks T (2008). Suppression of non-small cell lung tumor development by the let-7 microRNA family. Proc. Natl. Acad. Sci. U S A. 105, 3903–3908. [PubMed: 18308936]

Kumar MS, Lu J, Mercer KL, Golub TR, and Jacks T (2007). Impaired microRNA processing enhances cellular transformation and tumorigenesis. Nat. Genet. 39, 673–677. [PubMed: 17401365]

Kurita R, Suda N, Sudo K, Miharada K, Hiroyama T, Miyoshi H, Tani K, and Nakamura Y (2013). Establishment of immortalized human erythroid progenitor cell lines able to produce enucleated red blood cells. PLoS One 8, e59890. [PubMed: 23533656]

Lee YT, de Vasconcellos JF, Yuan J, Byrnes C, Noh SJ, Meier ER, Kim KS, Rabel A, Kaushal M, Muljo SA, et al. (2013). LIN28B-mediated expression of fetal hemoglobin and production of fetal-like erythrocytes from adult human erythroblasts ex vivo. Blood 122, 1034–1041. [PubMed: 23798711]

MacKinney AA Jr. (1978). Effect of aging on the peripheral blood lymphocyte count. J. Gerontol. 33, 213–216. [PubMed: 627705]

Manier S, Powers JT, Sacco A, Glavey SV, Huynh D, Reagan MR, Salem KZ, Moschetta M, Shi J, Mishima Y, et al. (2017). The LIN28B/let-7 axis is a novel therapeutic pathway in multiple myeloma. Leukemia 31, 853–860. [PubMed: 27773931]

McKinney-Freeman S, Cahan P, Li H, Lacadie SA, Huang HT, Curran M, Loewer S, Naveiras O, Kathrein KL, Konantz M, et al. (2012). The transcriptional landscape of hematopoietic stem cell ontogeny. Cell Stem Cell 11, 701–714. [PubMed: 23122293]

Mochizuki-Kashio M, Mishima Y, Miyagi S, Negishi M, Saraya A, Konuma T, Shinga J, Koseki H, and Iwama A (2011). Dependency on the polycomb gene Ezh2 distinguishes fetal from adult hematopoietic stem cells. Blood 118, 6553–6561. [PubMed: 22042701]

Moss EG, Lee RC, and Ambros V (1997). The cold shock domain protein LIN-28 controls developmental timing in C. elegans and is regulated by the lin-4 RNA. Cell 88, 637–646. [PubMed: 9054503]

Neo WH, Booth CAG, Azzoni E, Chi L, Delgado-Olguin P, de Bruijn M, Jacobsen SEW, and Mead AJ (2018). Cell-extrinsic hematopoietic impact of Ezh2 inactivation in fetal liver endothelial cells. Blood 131, 2223–2234. [PubMed: 29555646]

Palmer S, Albergante L, Blackburn CC, and Newman TJ (2018). Thymic involution and rising disease incidence with age. Proc. Natl. Acad. Sci. U S A 115, 1883–1888. [PubMed: 29432166]

Pang WW, Price EA, Sahoo D, Beerman I, Maloney WJ, Rossi DJ, Schrier SL, and Weissman IL (2011). Human bone marrow hematopoietic stem cells are increased in frequency and myeloid-biased with age. Proc. Natl. Acad. Sci. U S A 108, 20012–20017. [PubMed: 22123971]

Park IK, Qian D, Kiel M, Becker MW, Pihalja M, Weissman IL, Morrison SJ, and Clarke MF (2003). Bmi-1 is required for maintenance of adult self-renewing haematopoietic stem cells. Nature 423, 302–305. [PubMed: 12714971]

Rao S, Lee SY, Gutierrez A, Perrigoue J, Thapa RJ, Tu Z, Jeffers JR, Rhodes M, Anderson S, Oravecz T, et al. (2012). Inactivation of ribosomal protein L22 promotes transformation by induction of the stemness factor, Lin28b. Blood 120, 3764–3773. [PubMed: 22976955]

Rebel VI, Miller CL, Eaves CJ, and Lansdorp PM (1996a). The repopulation potential of fetal liver hematopoietic stem cells in mice exceeds that of their liver adult bone marrow counterparts. Blood 87, 3500–3507. [PubMed: 8605370]

Rebel VI, Miller CL, Thornbury GR, Dragowska WH, Eaves CJ, and Lansdorp PM (1996b). A comparison of long-term repopulating hematopoietic stem cells in fetal liver and adult bone marrow from the mouse. Exp. Hematol. 24, 638–648. [PubMed: 8605969]

Renshaw SA, Loynes CA, Trushell DM, Elworthy S, Ingham PW, and Whyte MK (2006). A transgenic zebrafish model of neutrophilic inflammation. Blood 108, 3976–3978. [PubMed: 16926288]

Rowe RG, Lummertz da Rocha E, Sousa P, Missios P, Morse M, Marion W, Yermalovich A, Barragan J, Mathieu R, Jha DK, et al. (2019). The developmental stage of the hematopoietic niche regulates lineage in MLL-rearranged leukemia. J. Exp. Med. 216, 527–538. [PubMed: 30728174]

Rowe RG, Mandelbaum J, Zon LI, and Daley GQ (2016a). Engineering hematopoietic stem cells: lessons from development. Cell Stem Cell 18, 707–720. [PubMed: 27257760]

Rowe RG, Wang LD, Coma S, Han A, Mathieu R, Pearson DS, Ross S, Sousa P, Nguyen PT, Rodriguez A, et al. (2016b). Developmental regulation of myeloerythroid progenitor function by the Lin28b-let-7-Hmga2 axis. J. Exp. Med. 213, 1497–1512. [PubMed: 27401346]

Saarinen UM, and Siimes MA (1978). Developmental changes in red blood cell counts and indices of infants after exclusion of iron deficiency by laboratory criteria and continuous iron supplementation. J. Pediatr. 92, 412–416. [PubMed: 632980]

Sato T, Kataoka K, Ito Y, Yokoyama S, Inui M, Mori M, Takahashi S, Akita K, Takada S, Ueno-Kudoh H, et al. (2020). Lin28a/let-7 pathway modulates the Hox code via Polycomb regulation during axial patterning in vertebrates. Elife 9, e53608. [PubMed: 32479258]

Shyh-Chang N, and Daley GQ (2013). Lin28: primal regulator of growth and metabolism in stem cells. Cell Stem Cell 12, 395–406. [PubMed: 23561442]

Skene PJ, and Henikoff S (2017). An efficient targeted nuclease strategy for high-resolution mapping of DNA binding sites. Elife 6, e21856. [PubMed: 28079019]

Smith LL, Yeung J, Zeisig BB, Popov N, Huijbers I, Barnes J, Wilson AJ, Taskesen E, Delwel R, Gil J, et al. (2011). Functional crosstalk between Bmi1 and MLL/Hoxa9 axis in establishment of normal hematopoietic and leukemic stem cells. Cell Stem Cell 8, 649–662. [PubMed: 21624810]

Tamburri S, Lavarone E, Fernandez-Perez D, Conway E, Zanotti M, Manganaro D, and Pasini D (2020). Histone H2AK119 mono-ubiquitination is essential for polycomb-mediated transcriptional repression. Mol. Cell 77, 840–856.e845. [PubMed: 31883952]

Taoudi S, Bee T, Hilton A, Knezevic K, Scott J, Willson TA, Collin C, Thomas T, Voss AK, Kile BT, et al. (2011). ERG dependence distinguishes developmental control of hematopoietic stem cell maintenance from hematopoietic specification. Genes Dev. 25, 251–262. [PubMed: 21245161]

Tober J, Maijenburg MMW, Li Y, Gao L, Hadland BK, Gao P, Minoura K, Bernstein ID, Tan K, and Speck NA (2018). Maturation of hematopoietic stem cells from prehematopoietic stem cells is accompanied by up-regulation of PD-L1. J. Exp. Med. 215, 645–659. [PubMed: 29282253]

Traver D, Paw BH, Poss KD, Penberthy WT, Lin S, and Zon LI (2003). Transplantation and in vivo imaging of multilineage engraftment in zebrafish bloodless mutants. Nat. Immunol. 4, 1238–1246. [PubMed: 14608381]

Tsuzuki S, Taguchi O, and Seto M (2011). Promotion and maintenance of leukemia by ERG. Blood 117, 3858–3868. [PubMed: 21321361]

Ustianenko D, Chiu HS, Treiber T, Weyn-Vanhentenryck SM, Treiber N, Meister G, Sumazin P, and Zhang C (2018). LIN28 selectively modulates a subclass of let-7 MicroRNAs. Mol. Cell 71, 271–283.e275. [PubMed: 30029005]

van den Boom V, Rozenveld-Geugien M, Bonardi F, Malanga D, van Gosliga D, Heijink AM, Viglietto G, Morrone G, Fusetti F, Vellenga E, et al. (2013). Nonredundant and locus-specific gene repression functions of PRC1 paralog family members in human hematopoietic stem/progenitor cells. Blood 121, 2452–2461. [PubMed: 23349393]

van Gent R, van Tilburg CM, Nibbelke EE, Otto SA, Gaiser JF, Janssens-Korpela PL, Sanders EA, Borghans JA, Wulffraat NM, Bierings MB, et al. (2009). Refined characterization and reference values of the pediatric T- and B-cell compartments. Clin. Immunol. 133, 95–107. [PubMed: 19586803]

Vanhee S, Akerstrand H, Kristiansen TA, Datta S, Montano G, Vergani S, Lang S, Ungerback J, Doyle A, Olsson K, et al. (2019). Lin28b controls a neonatal to adult switch in B cell positive selection. Sci. Immunol. 4, eaax4453. [PubMed: 31562190]

Vo LT, Kinney MA, Liu X, Zhang Y, Barragan J, Sousa PM, Jha DK, Han A, Cesana M, Shao Z, et al. (2018). Regulation of embryonic haematopoietic multipotency by EZH1. Nature 553, 506–510. [PubMed: 29342143]

Wang S, Chim B, Su Y, Khil P, Wong M, Wang X, Foroushani A, Smith PT, Liu X, Li R, et al. (2019). Enhancement of LIN28B-induced hematopoietic reprogramming by IGF2BP3. Genes Dev. 33, 1048–1068. [PubMed: 31221665]

Xie H, Xu J, Hsu JH, Nguyen M, Fujiwara Y, Peng C, and Orkin SH (2014). Polycomb repressive complex 2 regulates normal hematopoietic stem cell function in a developmental-stage-specific manner. Cell Stem Cell 14, 68–80. [PubMed: 24239285]

Young K, Borikar S, Bell R, Kuffler L, Philip V, and Trowbridge JJ (2016). Progressive alterations in multipotent hematopoietic progenitors underlie lymphoid cell loss in aging. J. Exp. Med. 213, 2259–2267. [PubMed: 27811054]

Young K, Eudy E, Bell R, Loberg MA, Stearns T, Sharma D, Velten L, Haas S, Filippi MD, and Trowbridge JJ (2021). Decline in IGF1 in the bone marrow microenvironment initiates hematopoietic stem cell aging. Cell Stem Cell 28 (8), 1473–1482. [PubMed: 33848471]

Yu H, Neale G, Zhang H, Lee HM, Ma Z, Zhou S, Forget BG, and Sorrentino BP (2014). Downregulation of Prdm16 mRNA is a specific antileukemic mechanism during HOXB4-mediated HSC expansion in vivo. Blood 124, 1737–1747. [PubMed: 25082879]

Yuan J, Nguyen CK, Liu X, Kanellopoulou C, and Muljo SA (2012). Lin28b reprograms adult bone marrow hematopoietic progenitors to mediate fetal-like lymphopoiesis. Science 335, 1195–1200. [PubMed: 22345399]

Zhou Y, Li YS, Bandi SR, Tang L, Shinton SA, Hayakawa K, and Hardy RR (2015). Lin28b promotes fetal B lymphopoiesis through the transcription factor Arid3a. J. Exp. Med. 212, 569–580. [PubMed: 25753579]

Zhu Q, Liu N, Orkin SH, and Yuan GC (2019). CUT&RUNTools: a flexible pipeline for CUT&RUN processing and footprint analysis. Genome Biol. 20, 192. [PubMed: 31500663]

Highlights

- Blood stem and progenitor cells are remodeled during development and maturation
- The *let-7* target, Cbx2, defines temporal blood stem and progenitor states
- Cbx2 controls expression of hematopoietic transcription factors during blood maturation

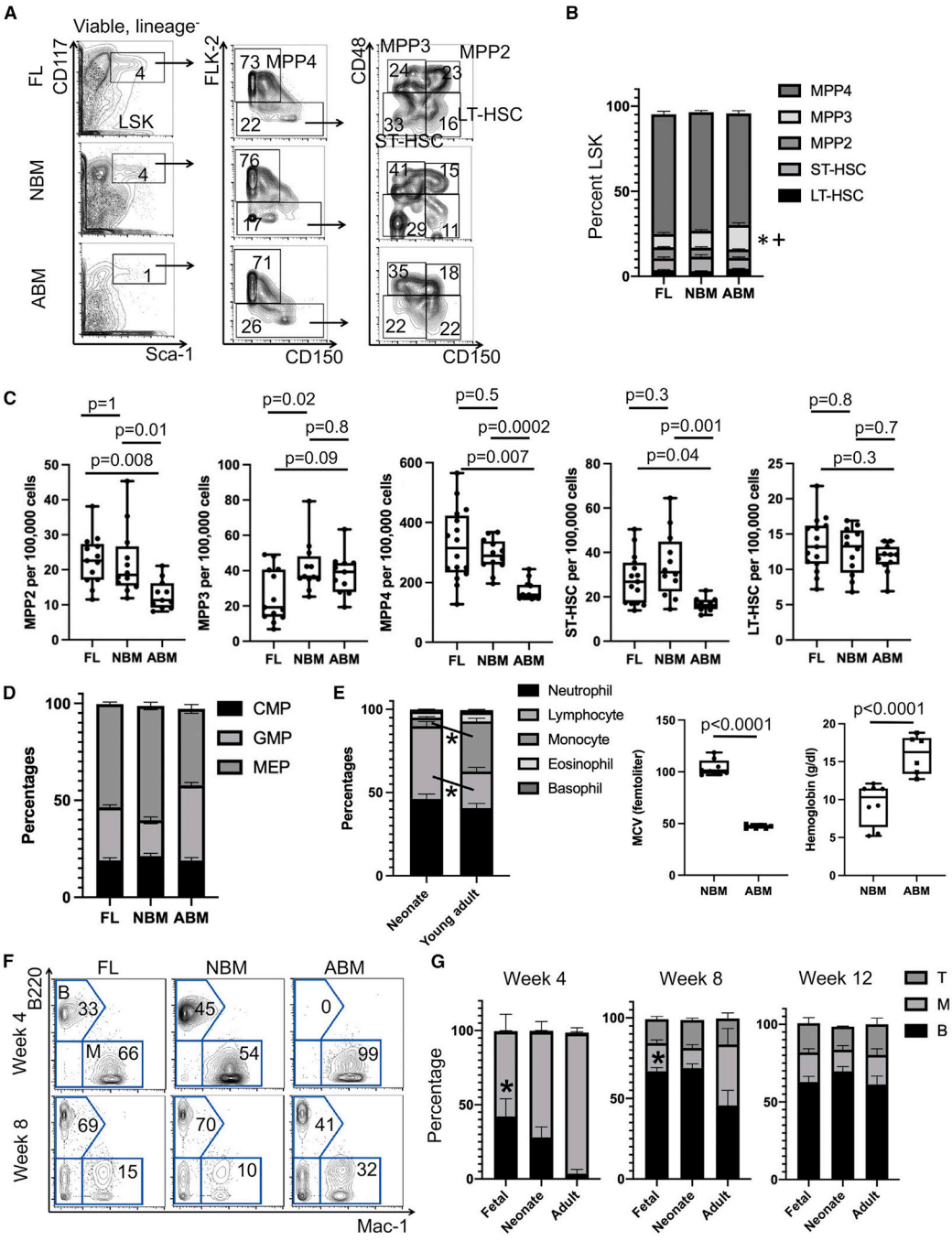

Figure 1. Developmental maturation of HSCs and MPPs

(A) Representative flow cytometry plots demonstrating distribution of HSCs and MPPs in E14.5 fetal liver (FL), P0–1 neonatal BM (NBM), and adult BM (ABM).

(B) Distribution of HSC and MPP populations as a percentage of viable Lineage$^-$ Sca-1$^+$ c-kit$^+$ (LSK) populations (*$p < 0.05$ compared with FL, + $p < 0.05$ compared with NBM by one-way ANOVA, mean ± SEM shown).

(C) Frequencies of various HSC and MPP populations per 100,000 viable cells in each hematopoietic organ. Results aggregated over three independent experimental cohorts.

Results depicted with box 25th–75th percentile range and whiskers entire data range, comparisons by one-way ANOVA with p values shown.

(D) Myeloid progenitor content as a percentage of viable Lineage- Sca-1^{-} c-kit^{+} (n = 18 FL, n = 6 NBM, n = 6 ABM collected over two experiments; $p < 0.01$ comparing each age with one another for granulocyte monocyte progenitors (GMPs) and megakaryocyte erythroid progenitors (MEPs); p = NS for common myeloid progenitors (CMPs). Statistical comparisons by one-way ANOVA.

(E) Peripheral blood parameters in NBM and ABM (n = 21 neonates, n = 9 adults; results aggregated over two independent experimental cohorts, *$p < 0.0001$ by Student's t test for the indicated comparisons for leukocyte populations; otherwise, p values shown), mean ± SEM shown..

(F) Representative flow cytometry profiles of the progeny of LT-HSCs from the indicated sources engrafted into congenic recipients at the indicated time points. Results representative of two independent experimental cohorts and mean ± shown..

(G) Quantification of the relative lineage output of LT-HSCs from the indicated ages at the indicated time points following transplantation into congenic recipients.

*$p < 0.05$ compared with adult by one-way ANOVA, mean ± SEM shown. Results aggregated over two independent transplantation experiments.

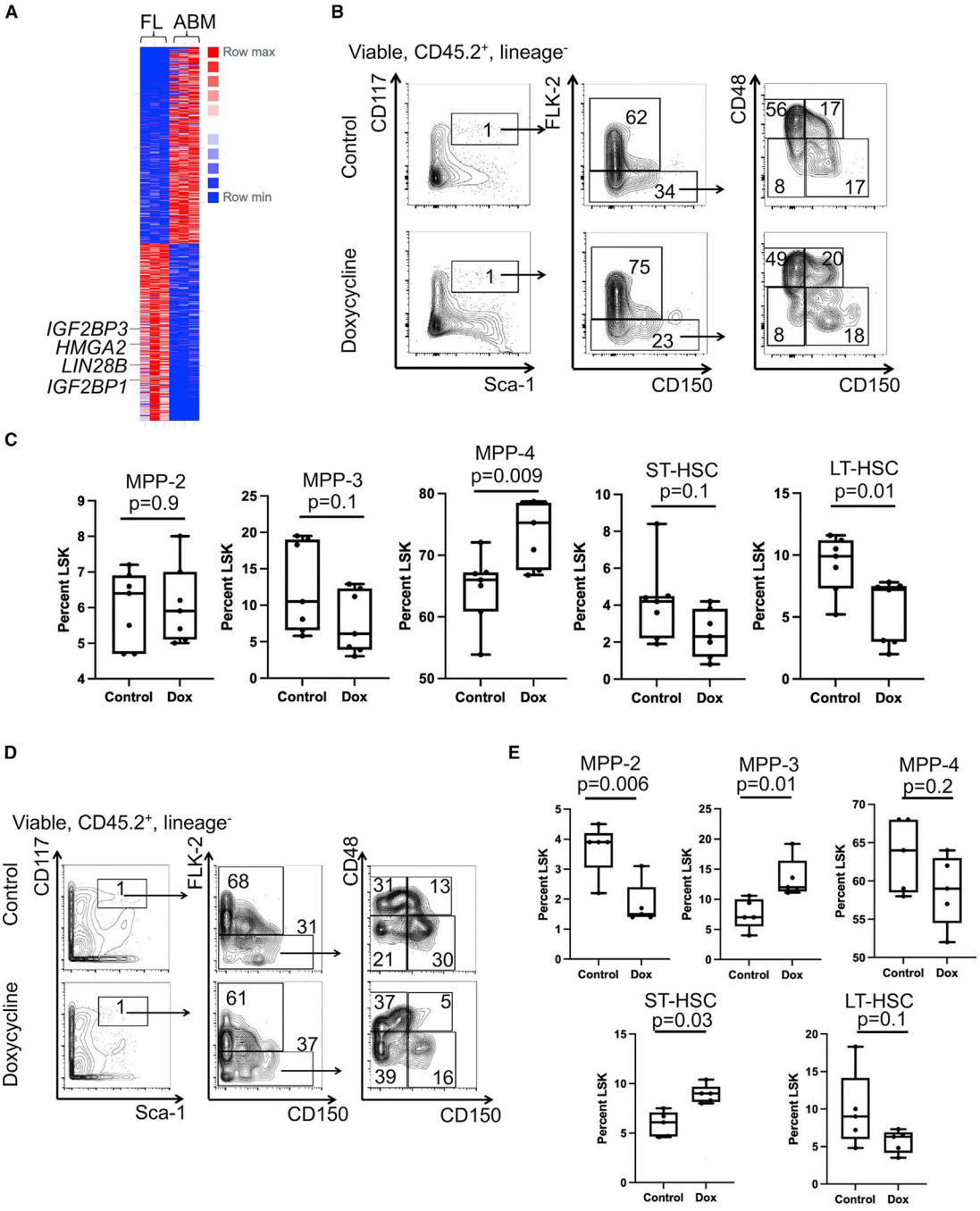

Figure 2. Regulation of HSC and MPP maturation by Lin28b and *let-7* microRNAs

(A) Heatmap demonstrating differential gene expression between FL and adult BM human HSCs (Cesana et al., 2018).

(B) Adult BM cells engineered for doxycycline-inducible LIN28B expression were transplanted into congenic recipients that were maintained with or without doxycycline in the drinking water. After 8 weeks, the distribution of HSCs and MPPs was examined in the donor-derived BM by flow cytometry.

(C) Quantification of the indicated HSC and MPP populations in control or doxycycline-treated mice at 8 weeks following transplantation. Results are aggregated over two independent experiments. Results depicted with box 25th–75th percentile range and whiskers entire data range, comparisons by unpaired t test with p values shown.
(D) Adult BM cells engineered for doxycycline-inducible, degradation-resistant *let-7g* expression were transplanted into congenic recipients that were maintained with or without doxycycline in the drinking water. After 8 weeks, the distribution of HSCs and MPPs was examined in the donor-derived BM by flow cytometry.
(E) Quantification of the indicated HSC and MPP populations in control or doxycycline-treated mice at 8 weeks following transplantation. Results depicted with box 25th–75th percentile range and whiskers entire data range, comparisons by unpaired t test with p values shown.

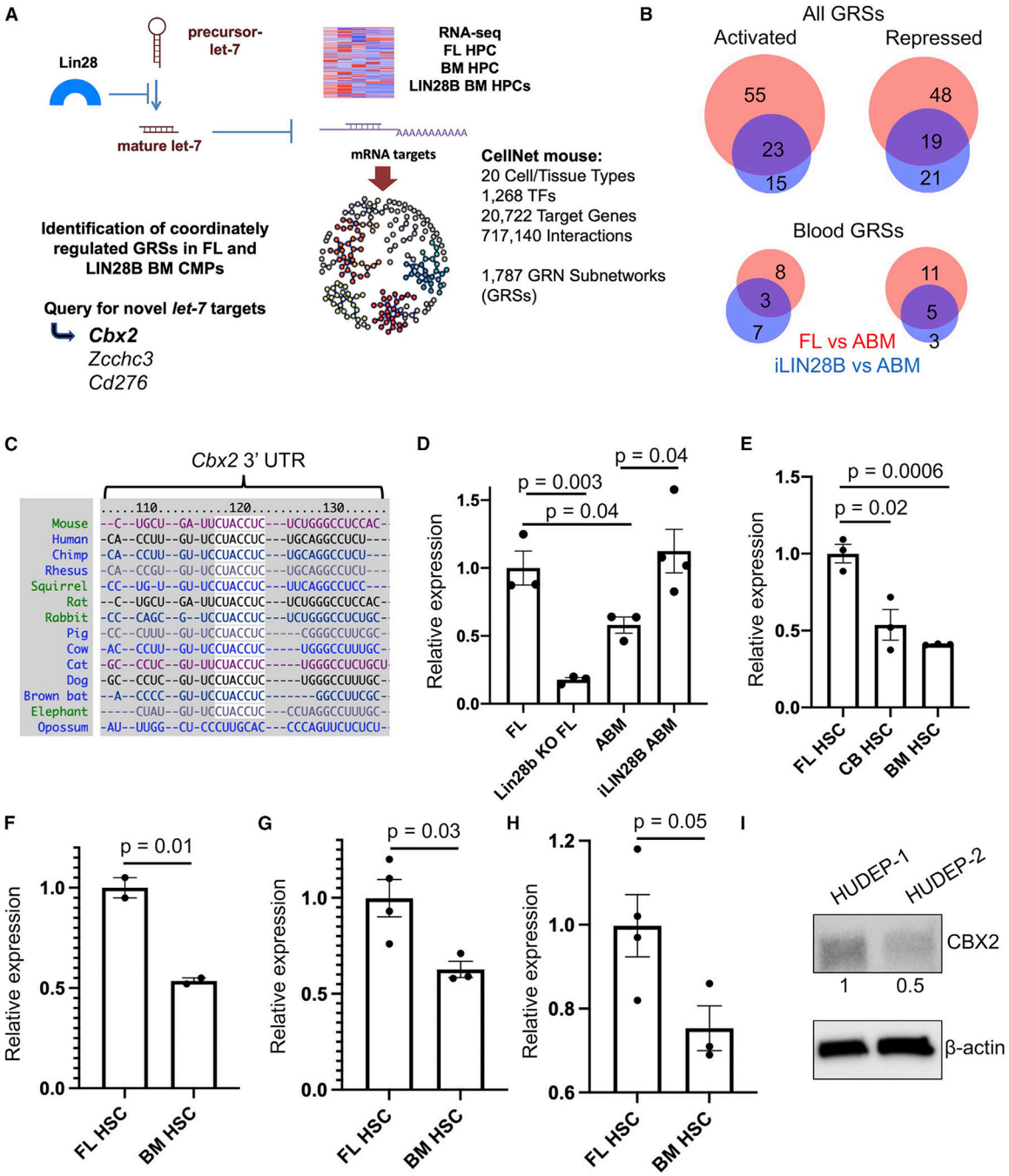

Figure 3. Cbx2 as a candidate developmentally regulated Lin28b/*let-7* target

(A) Approach to querying datasets for candidate GRSs that are developmentally regulated by Lin28b and that contain *let-7* target transcripts.

(B) Quantification of GRSs coordinately activated or repressed in E14.5 FL compared with ABM progenitors, or LIN28B-expressing ABM progenitors compared with wild-type ABM progenitors (Rowe et al., 2016b).

(C) Targetscan readout showing conservation of consensus *let-7* site in the 3′ untranslated region (UTR) of *Cbx2* across the indicated species.

(D) Quantification of *Cbx2* expression in the indicated common myeloid progenitor populations by RNA-seq (Rowe et al., 2016b). Results compared by unpaired t test, mean ± SEM and p value shown.

(E) Quantification of *CBX2* expression in the indicated human HSC populations by RNA-seq (Cesana et al., 2018). Results compared by unpaired t test, mean ± SEM and p values shown.

(F–H) Analysis of RNA-seq data of *Cbx2* expression in two subpopulations of murine FL HSCs compared with adult BM HSCs (F and G) (Beaudin et al., 2016) or in an independent dataset (H) (Chen et al., 2019; Tober et al., 2018). Results compared by unpaired t test, mean ± SEM and p value shown.

(I) Levels of CBX2 protein were measured by western blotting in HUDEP-1 (neonatal) and HUDEP-2 (adult) erythroid progenitor cells with quantification of band intensity normalized to β-actin loading control shown.

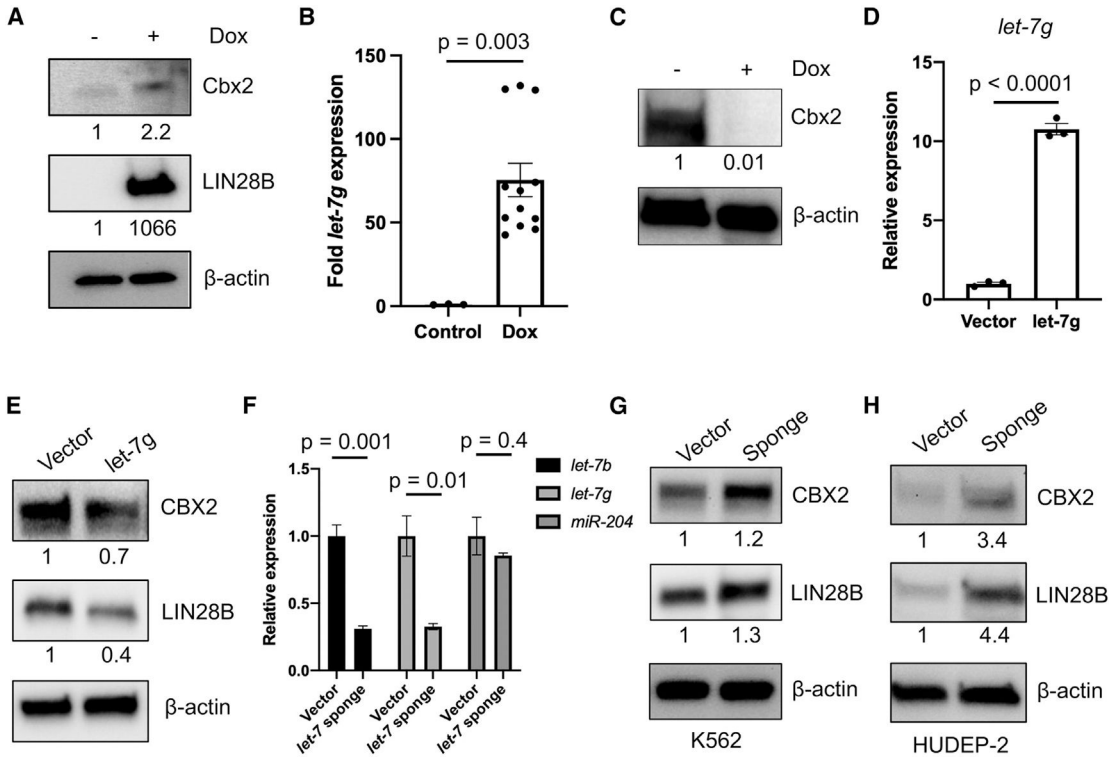

Figure 4. Regulation of Cbx2 by the Lin28b/*let-7* axis

(A) Adult mice (8 weeks old) bearing transgenes for doxycycline-inducible LIN28B expression were treated with or without doxycycline in the drinking water for 2 weeks, at which time western blotting was performed.

(B) Pregnant females bearing embryos with doxycycline-inducible *let-7g* expression were treated with doxycycline for 72 h leading up to harvesting of FLs at E14.5, at which time expression of *let-7g* was measured.

(C) Pregnant females with embryos bearing transgenes for doxycycline-inducible *let-7g* expression were treated with or without doxycycline in the drinking water from E11.5 to E14.5, at which time FLs were isolated and western blotting performed.

(D) Expression of *let-7g* was measured in K562 cells expressing the indicated constructs by quantitative RT-PCR.

(E) Levels of the indicated proteins were measured in K562 cells expressing the indicated constructs by western blotting.

(F) Levels of the indicated microRNA species were measured by quantitative PCR.

(G) Levels of the indicated proteins were measured in K562 cells expressing the indicated constructs by western blotting.

(H) HUDEP-2 cells expressing a control vector or *let-7* sponge were analyzed by western blotting. In all western blot panels, quantification of band intensity is normalized to the β-actin loading control shown. All statistical comparisons by unpaired Student's t test, with mean ± SEM and p values shown. All quantitative PCR experiments aggregated over three independent experiments.

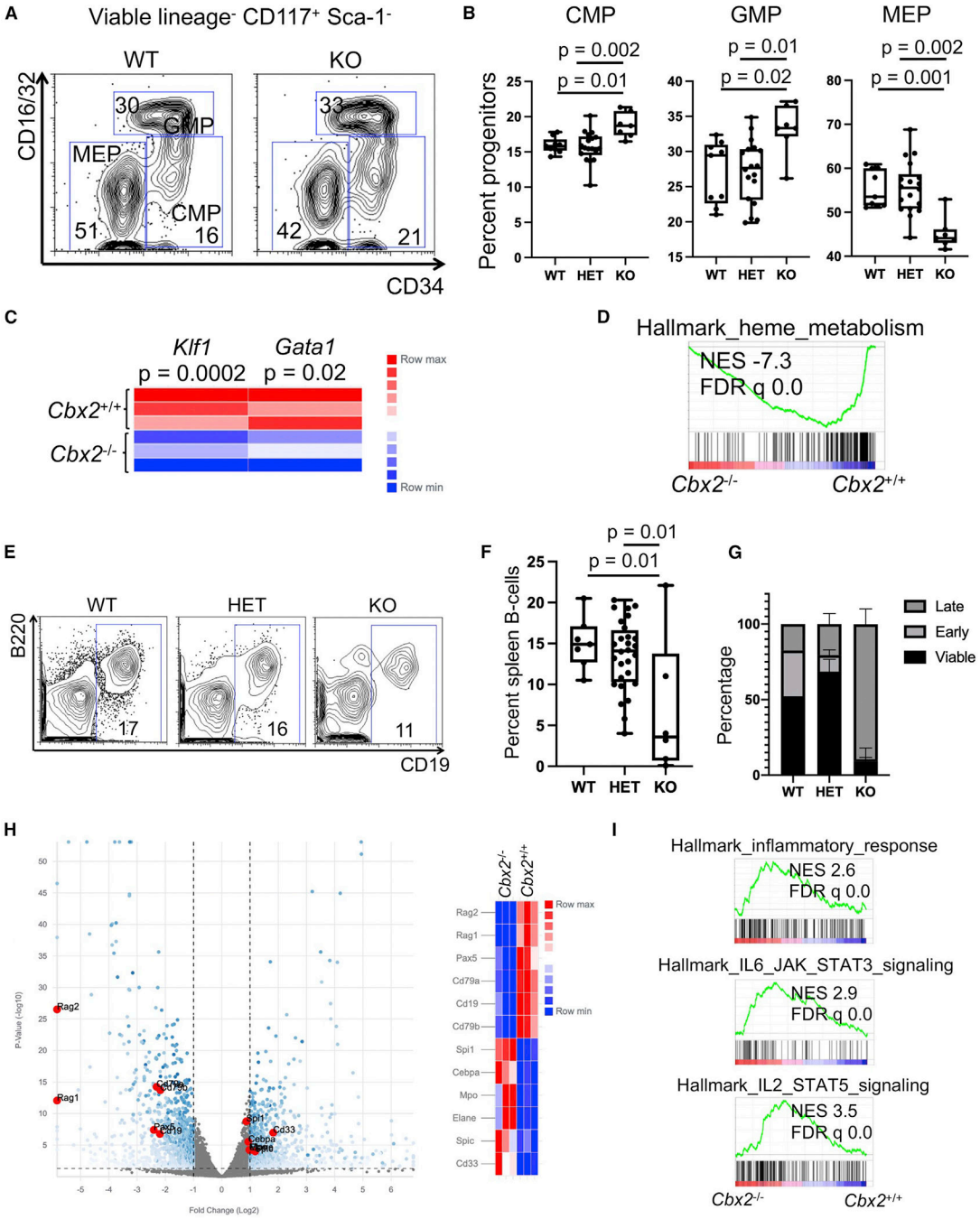

Figure 5. Regulation of juvenile hematopoiesis by Cbx2

(A) Representative flow cytometry plot of viable, lineage-c-kit^{+} Sca-1^{-} myeloerythroid progenitors from the indicated *Cbx2* genotypes.

(B) Quantification of myeloerythroid progenitors from the indicated genotypes. Results depicted with box 25th–75th percentile range and whiskers entire data range, comparisons by one-way ANOVA with p values shown.

(C) Heatmap showing expression of erythroid transcription factors in *Cbx2*$^{+/+}$ versus *Cbx2*$^{-/-}$ neonatal BM (Katoh-Fukui et al., 2019).

(D) Gene set enrichment analysis of *Cbx2*$^{+/+}$ versus *Cbx2*$^{-/-}$ neonatal BM (Katoh-Fukui et al., 2019).

(E) Representative flow cytometry plots of B cell markers in the P0 neonatal spleen of the indicated genotypes.

(F) Quantification of B220^{+} CD19^{+} mature B cells in the P0 neonatal spleen of the indicated genotypes. Results depicted with box 25th–75th percentile range and whiskers entire data range, comparisons by one-way ANOVA with p values shown.

(G) Quantification of CD19^{+} B cells either viable or in the early or late phases of apoptosis. HET viable compared with KO p = 0.0004, data are presented as mean ± SEM.

(H) Volcano plot and heatmap showing differentially expressed transcripts in *Cbx2*$^{+/+}$ versus *Cbx2*$^{-/-}$ neonatal BM (Katoh-Fukui et al., 2019).

(I) Gene set enrichment analysis of *Cbx2*$^{+/+}$ versus *Cbx2*$^{-/-}$ neonatal BM (Katoh-Fukui et al., 2019).

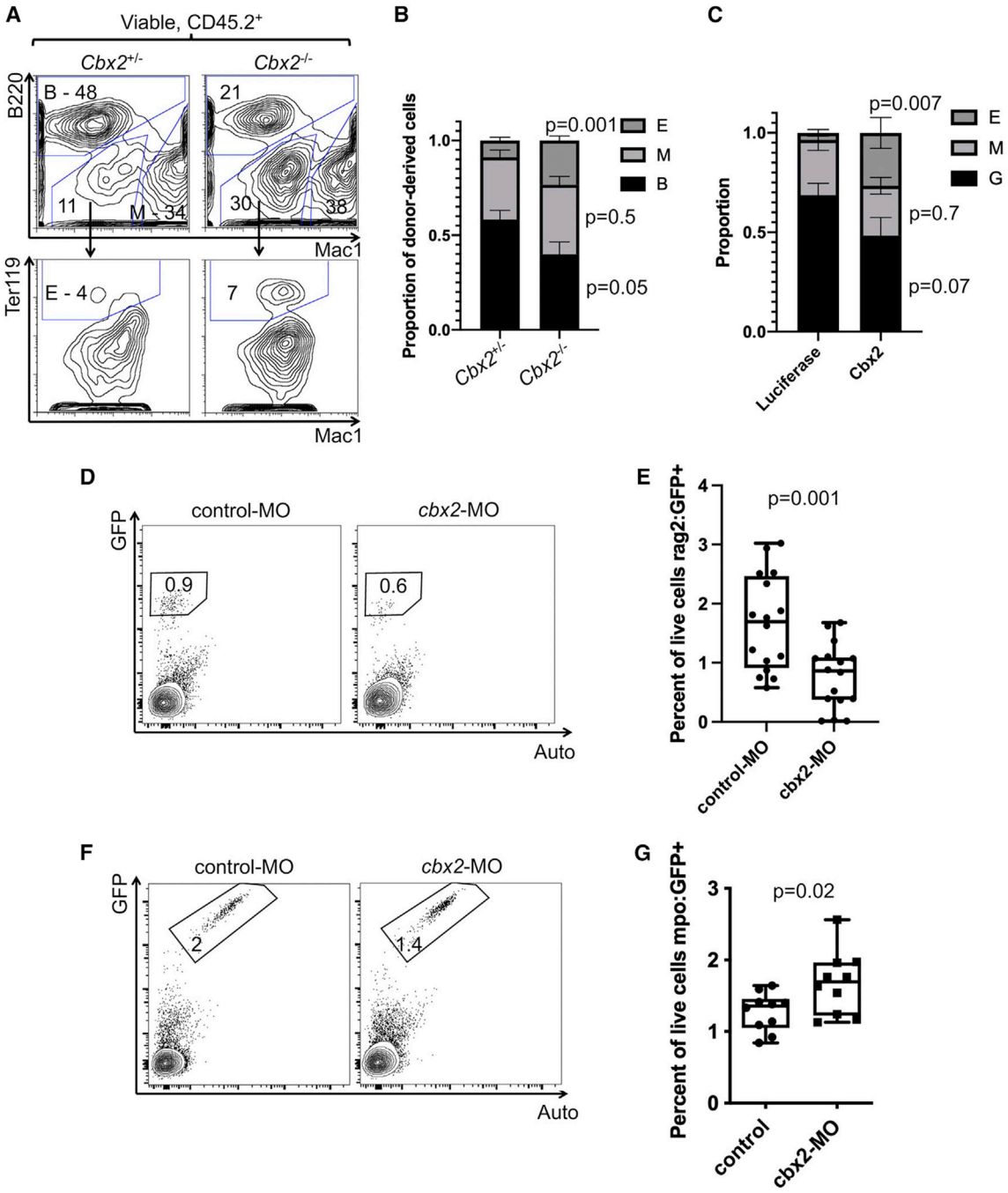

Figure 6. Regulation of lineage output by Cbx2

(A and B) MPP-4s from E14.5 FL were transplanted into congenic recipients. After 2 weeks, lineage output was analyzed (n = 5 recipients of *Cbx2*$^{+/-}$ or *Cbx2*$^{-/-}$ MPP-4 tested; E, erythroid; M, myeloid; B, B cell). Comparisons by unpaired Student's t test, data are presented as mean ± SEM with p values shown.

(C) Wild-type adult LSKs were transduced with the indicated vectors and plated in methylcellulose. GEMM colonies were picked and lineage output analyzed by flow cytometry (n = 14 luciferase and 12 Cbx2 colonies; E, erythroid; M, monocyte; G,

granulocyte lineage). Comparisons by unpaired Student's t test, data are presented as mean ± SEM with p values shown.

(D and E) Control or *cbx2* targeting morpholinos were introduced into *rag2:GFP* transgenic zebrafish embryos. At 96 h post fertilization, embryos were dissociated (five embryos pooled for each data point) and analyzed by flow cytometry. Results are pooled from two independent experiments. Results depicted with box 25th–75th percentile range and whiskers entire data range, comparisons by unpaired t test with p values shown.

(F and G) Control or *cbx2* targeting morpholinos were introduced into *mpo:GFP* transgenic zebrafish embryos. At 96 h post fertilization, embryos were dissociated (five embryos pooled for each data point) and analyzed by flow cytometry. Results are pooled from two independent experiments. Results depicted with box 25th–75th percentile range and whiskers entire data range, comparisons by unpaired t test with p values shown.

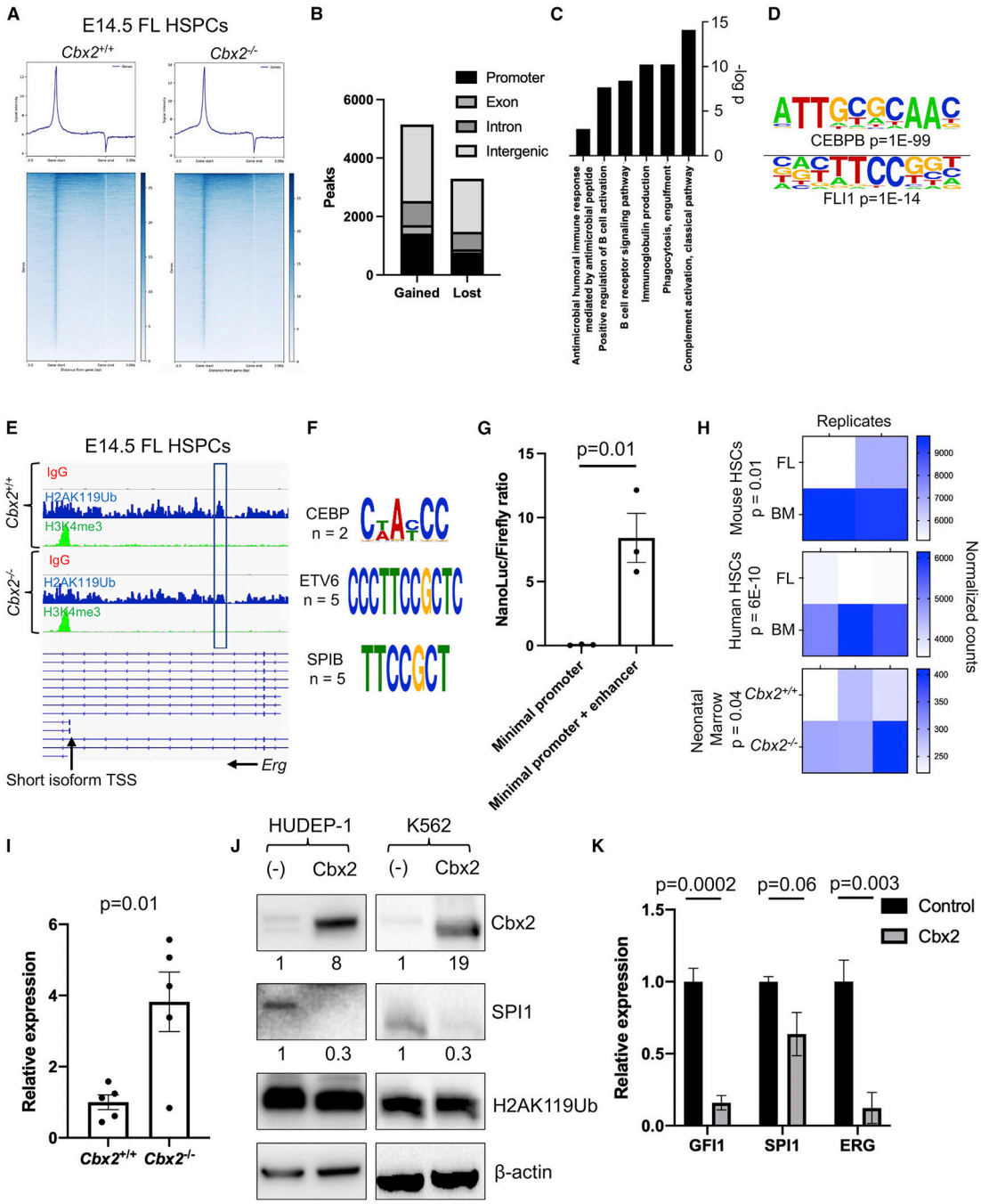

Figure 7. Control of juvenile hematopoiesis by Cbx2/PRC1

(A) CUT&RUN for H2AK119Ub in *Cbx2*$^{+/+}$ compared with *Cbx2*$^{-/-}$ E14.5 FL HSPCs showing distribution in gene bodies.

(B) H2AK119Ub CUT&RUN data were compared between *Cbx2*$^{+/+}$ and *Cbx2*$^{-/-}$ E14.5 FL HSPCs to identify differential peaks (n = 3 of each genotype isolated in three independent experiments).

(C) Gene ontology analysis of genes associated with peaks gained and lost in *Cbx2*$^{-/-}$ compared with *Cbx2*$^{+/+}$ HSPCs.

(D) HOMER analysis of motifs enriched in H2AK119Ub peaks lost in *Cbx2*$^{-/-}$ compared with *Cbx2*$^{+/+}$ HSPCs.

(E) CUT&RUN tracks for the indicated markers within the mouse *Erg* gene. Transcriptional start site of the short *Erg* isoform and the candidate enhancer region are indicated.

(F) Representative *cis* binding motifs for the indicated transcription factors identified in the candidate *Erg* enhancer.

(G) A fragment of the candidate *Erg* enhancer boxed in (E) was cloned into a vector with a minimal promoter driving expression of Nanoluc. This vector was cotransfected with a constitutive Firefly luciferase vector into K562 cells. Twenty-four hours later, Nanoluc and Firefly signals were quantified and expressed as a Nanoluc:Firefly ratio (n = 3 independent experiments).

(H) Heatmaps showing *ERG*/*Erg* expression in the indicated datasets by RNA-seq. p values are shown.

(I) Quantitative RT-PCR for *Erg* from neonatal spleens from the indicated genotypes normalized to actin.

(J) Western blotting for the indicated proteins in either control HUDEP-1 cells or cells transduced with a Cbx2 expression vector or K562 cells with or without Cbx2 expression from a doxycycline-inducible vector. Quantification of band intensity is normalized to the β-actin loading control shown.

(K) Quantitative RT-PCR for the indicated transcripts in either control HUDEP-1 cells or cells transduced with a Cbx2 expression vector. In all panels, results are presented as average ± SEM compared by Student's t test, with p values shown, aggregated over three independent experiments.

KEY RESOURCES TABLE

REAGENT or RESOURCE	SOURCE	IDENTIFIER
Antibodies		
Rabbit polyclonal anti-CBX2	Abcam	Cat#80044; RRID: AB_2049270
Rabbit polyclonal anti-CBX2	Bethyl	Cat#A302–524A; RRID: AB_1998943
Rabbit monoclonal anti-LIN28B	Cell Signaling Technology	Cat#11965; RRID: AB_2750978
Rabbit monoclonal anti-PU.1	Cell Signaling Technology	Cat#2258; RRID: AB_2186909
Rabbit monoclonal anti-Ubiquityl-Histone H2A (Lys119)	Cell Signaling Technology	Cat#8240; RRID: AB_10891618
Rabbit monoclonal anti-β-Actin	Cell Signaling Technology	Cat#4970; RRID: AB_2223172
B220-Pacific blue (RA3–6B2)	BioLegend	Cat#103227; RRID: AB_492876
B220-PE-Cy7 (RA3–6B2)	BioLegend	Cat#103222; RRID: AB_313005
CD117-APC-Cy7 (2B8)	BioLegend	Cat#105826; RRID: AB_1626278
CD150-APC (TC15–12F12.2)	BioLegend	Cat#115910; RRID: AB_493460
CD16/32-PerCP-Cy5.5 (93)	BioLegend	Cat#101324; RRID: AB_1877267
CD19-PE (eBio1D3)	eBioscience	Cat#12–0193-85; RRID: AB_657662
CD3-Pacific blue (17A2)	BioLegend	Cat#100214; RRID: AB_493645
CD3-PE (17A2)	BioLegend	Cat#100206; RRID: AB_312663
CD34-FITC (RAM34)	eBioscience	Cat#11–0341-85; RRID: AB_465022
CD45.1-APC-Cy7 (A20)	BioLegend	Cat#110716; RRID: AB_313505
CD45.2-FITC (104)	BioLegend	Cat#109806; RRID: AB_313443
CD48-FITC (HM48–1)	BioLegend	Cat#103404; RRID: AB_313019
CD5-APC-Cy7 (53–7.3)	BioLegend	Cat#100650; RRID: AB_2876396
Flk2-PE (A2F10)	BioLegend	Cat#135306; RRID: AB_1877217
Gr-1-Pacific blue (RB6–8C5)	BioLegend	Cat#108430; RRID: AB_893556
Mac-1-PE-Cy5 (M1/70)	BioLegend	Cat#101210; RRID: AB_312793
Sca-1-PE- Cy7 (D7)	BioLegend	Cat#108114; RRID: AB_493596
Ter119-APC-Cy7 (TER-119)	BioLegend	Cat#116223; RRID: AB_2137788
Ter119-Pacific blue (TER-119)	BioLegend	Cat#116232; RRID: AB_2251160
Chemicals, peptides, and recombinant proteins		
APC-annexin V	BioLegend	Cat#640919
Dexamethasone	Sigma-Aldrich	Cat#D4902
Doxycycline	Sigma-Aldrich	Cat#D9891
Geneticin™ Selective Antibiotic	Thermo Fisher Scientific	Cat# 10131035
Human EPO	PeproTech	Cat#500-P318
Human SCF	R&D	Cat#255-SC
Power SYBR™ Green PCR Master Mix	Thermo Fisher Scientific	Cat#4367659
SuperScript™ II Reverse Transcriptase	Thermo Fisher Scientific	Cat#18064
TRIzol™ Reagent	Thermo Fisher Scientific	Cat#15596026

REAGENT or RESOURCE	SOURCE	IDENTIFIER
Critical commercial assays		
CD117 MicroBeads, mouse	Miltenyi Biotec	Cat#130–091-224
CUTANA™ ChIC/CUT&RUN Kit	EpiCypher	Cat#14–1048
miScript II RT Kit	QIAGEN	Cat#218161
Nano-Glo® Dual-Luciferase® Reporter Assay System	Promega	Cat#N1610
SYTOX™ Blue Dead Cell Stain	Life Technologies	Cat#S34857
SYTOX™ Red Dead Cell Stain	Life Technologies	Cat#S34859
Deposited data		
Raw data	This paper	phs002507
Raw and analyzed data	This paper	GSE179160
Experimental models: Cell lines		
Human: HEK-293T	ATCC	RRID:CVCL_0045
Human: HUDEP-1	RIKEN	RRID:CVCL_VI05
Human: HUDEP-2	RIKEN	RRID:CVCL_VI06
Human: K562	ATCC	RRID:CVCL_0004
Experimental models: Organisms/strains		
Mouse: C57BL/6J	The Jackson Laboratory	JAX:000664
Mouse: B6.SJL-Ptprca Pepcb/BoyJ	The Jackson Laboratory	JAX: 002014
Mouse: B6Ei.129P2(C)-Cbx2tm1Cim/EiJ	The Jackson Laboratory	JAX: 006002
Mouse: iLet7	Rowe et al. (2016a)	N/A
Mouse: iLIN28B	Rowe et al. (2016b)	N/A
Zebrafish: Tg(rag2:GFP)	Traver et al. (2003)	ZFIN: ZDB-TGCONSTRCT-070117–56
Zebrafish: Tg(mpo:GFP)	Renshaw et al. (2006)	ZFIN: ZDB-ALT-070118–2
Oligonucleotides		
Splice-blocking morpholino oligonucleotides: cbx2: TAGTTTCCTGAGAGAGGAACACAAA	This paper	N/A
Primer for human CBX2: Forward: GACAGAACCCGTCAGTGTCC	This paper	N/A
Primer for human CBX2: Reverse: GGCTTCAGTAATGCCTCAGGT	This paper	N/A
Primer for human GAPDH: Forward: GTCTCCTCTGACTTCAACAGCG	This paper	N/A
Primer for human GAPDH: Reverse: ACCACCCTGTTGCTGTAGCCAA	This paper	N/A
Primer for human GFI1: Forward: GAGCCTGGAGCAGCACAAAG Reverse: GTGGATGACCTCTTGAAGCTCTTC	This paper	N/A
Primer for human GFI1: Reverse: GTGGATGACCTCTTGAAGCTCTTC	This paper	N/A
Primer for human SPI1: Forward: GACACGGATCTATACCAACGCC	This paper	N/A
Primer for human SPI1: Reverse: CCGTGAAGTTGTTCTCGGCGAA	This paper	N/A

REAGENT or RESOURCE	SOURCE	IDENTIFIER
Primer for human ERG: Forward: GGACAGACTTCCAAGATGAGCC Reverse: CCACACTGCATTCATCAGGAGAG	This paper	N/A
Primer for human ERG: Reverse: CCACACTGCATTCATCAGGAGAG	This paper	N/A
Primer for mouse b-Actin: Forward: ACGAGGCCCAGAGCAAGAGAGG Reverse: ACGCACCGATCCACACAGAGTA	This paper	N/A
Primer for mouse b-Actin: Reverse: ACGCACCGATCCACACAGAGTA	This paper	N/A
Primer for mouse Erg: Forward: GAGTGGGCGGTGAAAGAATA Reverse: TCAACGTCATCGGAAGTCAG	This paper	N/A
Primer for mouse Erg: Forward: Reverse: TCAACGTCATCGGAAGTCAG	This paper	N/A
Recombinant DNA		
pCW57.1	Gift from David Root	Addgene plasmid # 41,393
pGL4.50	Promega	Cat#E1310
pNL3.1	Promega	Cat#N1031
pNL3.1-Erg	This paper	N/A
pMSCV-neo let-7g	Kumar et al. (2007)	Addgene plasmid #14784
pMSCV-puro let-7 sponge	Kumar et al. (2007)	Addgene plasmid # 29,766
Software and algorithms		
CellNet algorithm	Cahan et al. (2014)	http://cellnet.hms.harvard.edu
CUT&RUNTools	Zhu et al. (2019)	http://broadinstitute.github.io/picard/
FlowJo	Becton, Dickinson and Company	https://www.flowjo.com/
HOMER	Feng et al. (2012)	http://liulab.dfci.harvard.edu/MACS
ImageJ	NIH	https://imagej.nih.gov/ij/
Targetscan algorithm	Agarwal et al. (2015)	http://www.targetscan.org/vert_80/